

UNCLASSIFIED

AD NUMBER

ADB001804

LIMITATION CHANGES

TO:

Approved for public release; distribution is unlimited.

FROM:

Distribution authorized to U.S. Gov't. agencies only; Test and Evaluation; 20 JAN 1975. Other requests shall be referred to Naval Air Systems Command, AIR - 954, Washington, DC 20361.

AUTHORITY

usnasc ltr, 12 apr 1976

THIS PAGE IS UNCLASSIFIED

THIS REPORT HAS BEEN DELIMITED  
AND CLEARED FOR PUBLIC RELEASE  
UNDER DOD DIRECTIVE 5200.20 AND  
NO RESTRICTIONS ARE IMPOSED UPON  
ITS USE AND DISCLOSURE.

DISTRIBUTION STATEMENT A

APPROVED FOR PUBLIC RELEASE;  
DISTRIBUTION UNLIMITED.

AD-B001804-L

①

BASIC ADHESION MECHANISMS IN THICK AND THIN FILMS

PRRL-74-CR-54

THOMAS T. HITCH AND KENNETH R. BUBE  
RCA LABORATORIES  
PRINCETON, NEW JERSEY 08540

31 JULY 1974

QUARTERLY TECHNICAL REPORT NO. 2  
For the Period 1 April 1974 to 30 June 1974

CONTRACT N00019-74-C-0270

D D C  
RECEIVED  
JAN 28 1975  
RECEIVED  
D

PREPARED FOR:  
NAVAL AIR SYSTEMS COMMAND  
WASHINGTON, D.C. 20361

DISTRIBUTION LIMITED TO U.S.  
GOVERNMENT AGENCIES ONLY;  
 FOREIGN INFORMATION  
 PROPRIETARY INFORMATION  
 TEST AND EVALUATION  
 CONTRACTOR PERFORMANCE EVALUATION

DATE: 1/20/75  
OTHER REQUESTS FOR THIS DOCUMENT  
MUST BE REFERRED TO COMMANDER,  
NAVAL AIR SYSTEMS COMMAND, AIR-954  
Washington, DC 20361

UNCLASSIFIED

SECURITY CLASSIFICATION OF THIS PAGE (When Date Entered)

REPORT DOCUMENTATION PAGE		READ INSTRUCTIONS BEFORE COMPLETING FORM
1. REPORT NUMBER	2. GOVT ACCESSION NO.	3. RECIPIENT'S CATALOG NUMBER
4. TITLE (and Subtitle) BASIC ADHESION MECHANISMS IN THICK AND THIN FILMS		5. TYPE OF REPORT & PERIOD COVERED Qtly. Technical No. 2 1-4-74 to 30-6-74
		6. PERFORMING ORG. REPORT NUMBER PRRL-74-CR-54
7. AUTHOR(s) Thomas T. Hitch Kenneth R. Bube		8. CONTRACT OR GRANT NUMBER(s) N00019-74-C-0270
9. PERFORMING ORGANIZATION NAME AND ADDRESS RCA Laboratories Princeton, NJ 08540		10. PROGRAM ELEMENT, PROJECT, TASK AREA & WORK UNIT NUMBERS
11. CONTROLLING OFFICE NAME AND ADDRESS Naval Air Systems Command Washington, D.C.		12. REPORT DATE 31 July 1974
		13. NUMBER OF PAGES 71
14. MONITORING AGENCY NAME & ADDRESS (if different from Controlling Office)		15. SECURITY CLASS. (of this report) Unclassified
		15a. DECLASSIFICATION/DOWNGRADING SCHEDULE N/A
16. DISTRIBUTION STATEMENT (of this Report)		
<p style="text-align: center;"><del>DISTRIBUTION LIMITED TO U.S. GOVERNMENT AGENCIES ONLY;</del></p> <p style="text-align: center;"><input type="checkbox"/> FOREIGN INFORMATION <input type="checkbox"/> PROPRIETARY INFORMATION <input checked="" type="checkbox"/> TEST AND EVALUATION <input type="checkbox"/> CONTRACTOR PERFORMANCE EVALUATION</p>		
17. DISTRIBUTION STATEMENT (of the abstract entered in Block 20, if different from Report)		
18. SUPPLEMENTARY NOTES DATE: 1/20/75 OTHER REQUESTS FOR THIS DOCUMENT MUST BE REFERRED TO COMMANDER, NAVAL AIR SYSTEMS COMMAND, AIR-954		
19. KEY WORDS (Continue on reverse side if necessary and identify by block number) Washington, DC 20361 Adhesion, bondability, gold conductors, gold powders, thick films, chemical analyses, reliability, sheet resistance, peel adhesion testing.		
20. ABSTRACT (Continue on reverse side if necessary and identify by block number) During this quarter, an historical overview of ceramic metallization was undertaken. This included a review of the applications of the technology prior to its utilization in hybrid microcircuits per se. The existing metal-to-ceramic bonding concepts were examined. Appropriate sintering models will be utilized in studying the fundamental aspects of gold thick-film adhesion in the next quarter. In conjunction with this, the inorganic chemical analyses of 17 commercial inks were completed. Furthermore, the		

DD FORM 1473  
1 JAN 73

EDITION OF 1 NOV 65 IS OBSOLETE

UNCLASSIFIED

SECURITY CLASSIFICATION OF THIS PAGE (When Date Entered)

UNCLASSIFIED

SECURITY CLASSIFICATION OF THIS PAGE(When Data Entered)

20.

microstructures of unfired inks have been examined by scanning electron microscopy and have disclosed gold in spherical and hexagonal-triangular platelet form. These data will enhance our understanding of gold-glass frit and gold-transition metal oxide bonding mechanisms. In addition, the physical and electrical properties of the 17 inks have been characterized on 96 and 99.5 wt pct alumina substrates. This primary parametric study included a ranking of ink performance in terms of printing resolution, adhesion strength (via the peel test method), and electric sheet resistance ( $\Omega$ /square). In terms of absolute failure load, one reactively bonded gold film exceeded that of all frit-bonded systems. This advantage was maintained even after multiple firing of the film and can be an important property in complex multilevel circuit applications. The lowest sheet resistance, approximately 2 m $\Omega$ /square, was found in a spherical gold powder-based frit-bonded ink. The remainder ranged in sheet resistance between 3 and 8 m $\Omega$ /square. With these basic properties established, the way is clear for a more intensive parametric study of the better inks during the next quarter.

UNCLASSIFIED

SECURITY CLASSIFICATION OF THIS PAGE(When Data Entered)

## PREFACE

This report describes work performed in the Process and Applied Materials Research Laboratory of RCA Laboratories under Contract No. N00019-74-C-0270. P. Rappaport is the Laboratory Director and G. L. Schnable is the Project Supervisor and Group Head. J. Willis is the Government Project Monitor.

It is a pleasure to acknowledge the help of a number of individuals who have contributed to this work by the performance of several analytical techniques. Notable are H. H. Whitaker - atomic absorption and optical emission spectrometry; B. L. Goydish - wet chemistry; E. M. Botnick - solids mass spectrometry; and G. R. Auth and B. J. Seabury - scanning electron microscopy.

We acknowledge the diligence and care of W. I. Rogers in the adhesion and sheet resistance testing. We further acknowledge the able assistance of E. J. Conlon in the preparation of samples for analysis in the development of the lead frame process, and in the day-to-day pursuit of the study. G. L. Schnable's review of the manuscript was particularly helpful.

The continued encouragement of and helpful discussions with G. L. Schnable, and the support of P. Rappaport in this work are much appreciated.

## TABLE OF CONTENTS

Section	Page
I. INTRODUCTION . . . . .	9
II. BACKGROUND OF METAL-CERAMIC INTERFACE TECHNOLOGY . . . . .	10
A. Introduction . . . . .	10
B. Metal-Ceramic Bonding Theories . . . . .	14
C. Sintering Models . . . . .	16
III. PROGRESS OF THE CONTRACT STUDY . . . . .	21
A. Chemical Analyses of Gold Pastes . . . . .	21
B. Adhesion and Conductivity Measurements . . . . .	28
1. Sample Preparation . . . . .	28
2. Experimental Procedures . . . . .	35
3. Results . . . . .	37
C. Adhesion Tests . . . . .	39
D. Ink Solids Study . . . . .	48
E. Discussion of Results - Properties of the Inks Studied . . . . .	60
IV. WORK TO BE DONE IN THE NEXT PERIOD . . . . .	63
APPENDIX A - DETAILS OF EXPERIMENTAL TECHNIQUE. . . . .	64
1. Fabrication of Gold Lead Frames. . . . .	64
2. Test Substrate Printing. . . . .	64
3. Substrate Firing . . . . .	65
REFERENCES. . . . .	67

## LIST OF ILLUSTRATIONS

Figure	Page
1. A block diagram of the first parametric study . . . . .	24
2. (a) Conductor test pattern, (b) frame to match conductor pattern in (a). . . . .	31
3. Belt furnace temperature profiles used in the study . . . . .	33
4. The RCA peel test (nominally after Ref. 71) . . . . .	36
5. Sheet resistance for 17 inks: (a) reactively and mixed- bonded gold inks, (b) frit-bonded inks containing 90 to 97 wt pct gold, and (c) other frit-bonded inks . . . . .	38
6. Adhesion data for several inks, substrates, and firings of reactively bonded and mixed bonded conductors . . . . .	45
7. Adhesion test data for the frit-bonded inks . . . . .	47
8. Adhesion test data for the heavily frit-bonded inks . . . . .	49
9. SEMograph of inorganic solids from ink A - 1. . . . .	50
10. SEMograph of inorganic solids from ink A - 2. . . . .	50
11. SEMograph of inorganic solids from ink B - 1. . . . .	51
12. SEMograph of inorganic solids from ink B - 2. . . . .	51
13. SEMograph of inorganic solids from ink C - 1. . . . .	52
14. SEMograph of inorganic solids from ink C - 2. . . . .	52
15. SEMograph of inorganic solids from ink C - 3. . . . .	53
16. SEMograph of inorganic solids from ink D - 1. . . . .	54
17. SEMograph of inorganic solids from ink D - 2. . . . .	54
18. SEMograph of inorganic solids from ink E - 1. . . . .	55
19. SEMograph of inorganic solids from ink E - 2. . . . .	55
20. SEMograph of inorganic solids from ink F - 1. . . . .	56
21. SEMograph of inorganic solids from ink F - 2. . . . .	56
22. SEMograph of inorganic solids from ink F - 3. . . . .	57

LIST OF ILLUSTRATIONS (Cont'd)

Figure	Page
23. SEMograph of inorganic solids from ink G - 1. . . . .	58
24. SEMograph of inorganic solids from ink G - 2. . . . .	58
25. SEMograph of inorganic solids from ink H - 1. . . . .	59

## LIST OF TABLES

Table	Page
1. Summary of Manufacturers' Data on Inks. . . . .	22
2. Chemical Analyses of 17 Gold Conductor Inks (Proportions shown in wt pct of inorganic solids.) . . . . .	25
3. Simplification of the Chemical Analysis Data for Thick-Film Gold Conductors Grouped by Binder Type. . . . .	29
4. Notes on the Printing Characteristics of Gold Thick Film. . . . .	32
5. Gold Thick-Film Drying and Firing Process Parameters. . . . .	34
6. Adhesion Data . . . . .	40

## I. INTRODUCTION

In the second quarter of the study "Basic Adhesion Mechanisms in Thick and Thin Films," we have nearly completed the parametric evaluation of the adhesion of 17 state-of-the-art gold inks on 96 and 99.5 wt pct alumina substrates. A second study will soon begin to determine the effects of additional process parameters on the adhesion of a smaller number of materials. Microstructural evaluations of fired samples from the first parametric study have been initiated. These will permit more detailed analyses of the adhesion strengths reported here.

Other work performed during this quarter included a review of the literature pertaining to glass-to-metal and ceramic-to-metal seals, and other ceramic metallizers. Such an approach is a broader attack on the subject of thick-film metallizers than is common. However, the older, established technology of seals and metallizers has much to offer thick-film hybrid technology. The review is given in Section II.

## II. BACKGROUND OF METAL-CERAMIC INTERFACE TECHNOLOGY

### A. INTRODUCTION

The art of metallizing ceramics probably began at least as early as the 19th century. Without attempting to trace the complete chronology of the matter, however, it was possible to obtain a broad overview by searching the recorded literature in Science Abstracts and elsewhere for the period 1954 - 1974. In today's terminology, ceramic metallization can be loosely divided into one of several classifications, i.e., a) "thin film" or vacuum techniques, b) chemical depositions or other methods such as electroplating, chemical vapor deposition, or flame spraying, and c) "thick film" or sintered metal methods.

Thin-film and chemical-deposition technologies have been widely utilized by the microelectronics industry, and numerous excellent review texts and articles have been published in this area. Details of metal evaporation, sputtering, and chemical vapor deposition can be found in works by Berry et al.,<sup>1</sup> Maissel and Glang,<sup>2</sup> Gregor,<sup>3</sup> Mattox,<sup>4</sup> and Vossen.<sup>5</sup> It is interesting to note that the entire question of assessing metal-to-ceramic adhesion is hardly unified in these advanced technologies. For example, Chapman<sup>6</sup> and Williams<sup>7</sup> have outlined numerous attempts for measuring "adhesion" and include test descriptions of scratch, pull, topple, and peel methods but offer little encouragement for believing that the problem is completely solved. In recent work on evaluating chromium-glass adhesion, Poley and Whitaker<sup>8</sup> describe a dynamic peel test method closely allied to the test of first choice in the present study. However, the pure tensile test is still being used.<sup>9</sup>

With specific regard to the application of gold to insulating oxide surfaces, Mattox<sup>10</sup> and Moore and Thornton<sup>11</sup> have found that simply increasing the ambient oxygen pressure will cause gold to adhere. However, it is generally recognized that metals with a greater affinity for oxygen are necessary to bridge the metal-oxide gap. This approach relies on thermodynamic considerations and the free energy of formations of stable metal oxides such as  $\text{CrO}_3$ ,  $\text{TiO}_2$ ,  $\text{SiO}_2$ , etc. On the other hand, metals with excessively large free energies of oxide formation, e.g., Ta, have been

found to cause poor adherence of Au-Ta on an oxide substrate by virtue of oxygen diffusion through the gold film. The resulting oxide, in this case  $Ta_2O_5$ , disrupts the Au-Ta interface.<sup>12</sup> In addition to the chemical bonding contribution to metal-insulator adhesion, other investigators<sup>13,14</sup> have shown an electrostatic component to be an important factor.

Intermediate between "thin" and "thick" film technologies, is the high-pressure, high-temperature method of bonding metals to ceramics. This has been reported by Calow and others<sup>15,16</sup> for the bonding of nickel, chromium, and Ni-Cr alloy sheets and nickel powder compacts to alumina. Indeed, Klomp<sup>17</sup> has extended this technique and bonded bulk Pb, Al, Cu, Ni, Fe, and Pt. The ceramic-metal bond strength was shown by Klomp to be proportional to the metal melting point. In the case of Cr and Ni-Cr alloys Calow<sup>16</sup> claims the strength derives from the solid solution of chromia in alumina, although no evidence is presented to support this. On the other hand, the spinel,  $NiAl_2O_4$ , was found in some cases where no bonding occurred in the nickel-alumina bond studies.<sup>15</sup> This implies that excessive reaction times can degrade the bond strength by the formation of weaker intermediate phases.

The bulk of the microelectronic hybrid circuit industry currently utilizes thick film or sintered-"fired-on" metallization. This method of fabricating hybrid integrated circuits promises to grow in the future as its functional and economic advantages become more widely accepted. There are several review texts available to acquaint the reader with this dynamic technology, and the works of Hamer and Biggers,<sup>18</sup> Miller,<sup>19</sup> and Topfer<sup>20</sup> are notable. Additionally, a great deal of detailed information can be gleaned from the annual published proceedings of the International Society for Hybrid Microelectronics Symposium and the IEEE/EIA Electronic Components Conference.

The current use of precious metal metallization systems grew out of the early use of ceramic capacitor and electron tube glass/ceramic-to-metal seal technology which began in the 1930's.<sup>18</sup> In developing a basis for discussing adhesion mechanisms, it is instructive to review the methodology

and materials which were used in these components. Reviews in this area have been published by Burnside (1954),<sup>21</sup> Van Houten (1959),<sup>22</sup> Clarke et al. (1965),<sup>23</sup> Kohl (1967),<sup>24</sup> and Pattee (1968).<sup>25</sup> These will be drawn on and supplemented to develop the existing concepts of ceramic-to-metal bonding.

The first intensive use of ceramic-to-metal sealing is generally credited to Pulfrich,<sup>26-29</sup> and his work in the 1930's still forms the basis for what is used today. His method consisted of coating the ceramic with finely divided molybdenum and iron powder and firing the coated assemblies in a controlled atmosphere and temperature range. Following this, the body was electroplated and brazed to the metal component. The conditions which were considered essential for vacuum-tight joints included close control of the physical and chemical properties of the metallizing metal and ceramic. In order for the metallizing metal to sinter to the proper porosity for mechanical interlocking, its melting point had to be about 200°C above the firing temperature. Additionally, an atmosphere which converted a small amount of molybdenum metal to the oxide was necessary to promote wetting of the ceramic. The ceramic must form a eutectic bond with the resultant metal oxide about 200°C below the metallizer sintering temperature. This eutectic melting temperature must, of course, be well below the softening temperature of the ceramic. Obviously, the metallized ceramic and the metal to which it was ultimately joined should have closely matching thermal coefficients of expansion. Any brazing filler metals must flow below the lowest ceramic eutectic temperature and not react adversely with the metallizing metal.

Following this initial application, additional variations of ceramic metallizing were developed, and Clarke et al.<sup>23</sup> cite coatings of

- a) metal/glass powder
- b) metal/metal oxide powder
- c) refractory-metal salt
- d) refractory-metal-oxide powder

A great number of metallizers were subsequently examined. Nolte and Spurck (1950)<sup>30</sup> found Mn-Mo gave more consistent strengths than Fe-Mo systems. In

work by Cole et al.<sup>31</sup> 200 formulations were tested and included various proportions and combinations of powdered Mo, W, Ti, Fe, Cu, Ni, Si,  $\text{Li}_2\text{CO}_3$ ,  $\text{ZrO}_2$ ,  $\text{MgO}$ ,  $\text{BaO}$ ,  $\text{CaO}$ ,  $\text{MoO}_3$ ,  $\text{WO}_3$ ,  $\text{TiO}_2$ ,  $\text{Fe}_2\text{O}_3$ , feldspar and other compounds. Adhesion strengths were measured on alumina substrates of three purities, i.e., 94%, 96%, and 99.6%. Values as high as 28,400-psi tensile strength were reported for the 94% aluminum body, and strengths were noted to decline with increasing alumina purity. The strongest formulations proved to be molybdenum/manganese mixtures with additions of silica or titanium. Helgesson,<sup>32</sup> on the other hand, found greater seal strengths in the Mo-Mn system with higher alumina content in the ceramic body.

Grimm and Strubhar<sup>33</sup> successfully metallized sapphire and beryllia with mixtures containing Mo/Mn and additions of "steatite-type" frit. Strengths of the metallized ceramic seals approached and in some cases equaled the substrate strengths.

Tungsten metallized 94% alumina bodies, with bond strengths of 12,000 psi, have been reported by Varadi and Dominquez.<sup>34</sup> In thermionic converters, containing cesium vapor, a special cesium-resistant yttria/tungsten metallizer was successfully formulated for use at  $1500^\circ\text{C}$ .<sup>35-39</sup> On 99.5% and 96%  $\text{Al}_2\text{O}_3$  bodies, room-temperature strengths of the order of 20,000 psi were reported when 2%  $\text{Y}_2\text{O}_3$  was added to tungsten.<sup>38</sup> Tentarelli et al.<sup>39</sup> found a 94% W-5% Mn-1% Fe mixture that yielded around 20,000-psi tensile strength when fired on 94%  $\text{Al}_2\text{O}_3$  bodies at  $1100^\circ\text{C}$ .

There is a large difference in the adhesion strengths of refractory and noble metal metallizers. Hoffman,<sup>40</sup> for example, reports only 1200-psi tensile strength for a Pt-Au glaze composition when fired on 96%  $\text{Al}_2\text{O}_3$  bodies. Crossland and Hailes,<sup>41</sup> in studying adhesion strengths on Pt-Au, Pd-Ag, and Pd-Au metallizers, found tensile strengths no higher than 4000 psi.

Metallization adhesion strength was also shown to be affected by other factors such as substrate characteristics. Floyd,<sup>42</sup> in examining Mo-Mn-to- $\text{Al}_2\text{O}_3$  substrate adhesion strength, showed improved strength with increasing  $\text{Al}_2\text{O}_3$  grain size. Additionally, flux composition and firing temperature affected metallization adhesion strength. By proper choice of flux composition, alumina particle size control, and firing temperature, strengths as high as 13,000 psi were obtained. Arthur and Fussell<sup>43</sup> also

found strength varied with the hydrogen content in the atmosphere during tests on Mo-Mn-to- $\text{Al}_2\text{O}_3$  seals. Klomp and Botden<sup>44</sup> have also shown  $\text{Al}_2\text{O}_3$ -to-Mo strengths of 24,000 psi, when fired in the presence of a frit containing various proportions of  $\text{Al}_2\text{O}_3$ , MnO and  $\text{SiO}_2$ .

#### B. METAL-CERAMIC BONDING THEORIES

From the briefly covered field of metallized ceramic technology, one can surmise that factors suspected of influencing adhesion have been abundantly sifted and evaluated. Before reviewing bonding theories it will be beneficial to cite some of the important variables. This might suppress our urge to generalize about all metal-ceramic systems. Clarke's<sup>23</sup> summary of variables is broad enough to cover the essence of it and is outlined as follows:

1. Temperature
2. Time.
3. Ceramic and metal compositions
  - a) Primary phases or major constituents
  - b) Grain boundary impurities
  - c) Lattice impurities
4. Grain size and orientation
5. Surface roughness
  - a) From deformation of the surface
  - b) From chemical attack of the surface
6. Lattice structure
  - a) Spacing of atoms and associated fields in crystalline planes
  - b) Imperfections (including impurities) distorting the lattice and/or leaving vacant sites
7. Surface contamination
  - a) Particles sitting on the surface
  - b) Adsorbed films and particles
8. Stresses
  - a) Resulting from thermal expansion differences
  - b) Epitaxially induced

Any attempt at developing a unified bonding theory must necessarily address at least these factors. However, investigators have attempted to explain bonding on the basis of observed systems. Thus, technology was

typically leading science's understanding of what promoted adhesion and why it performed well in some applications and poorly in others.

Historically, several "theories" were developed and began with Pincus's<sup>45</sup> view of the Mo-Mn systems. He postulated a chemical reaction between the substrate alumina and the oxidized Mn from the metallization. This reaction resulted in the formation of manganese aluminate spinel. He expanded on this to include reactions between  $\text{Al}_2\text{O}_3$  and Mo to yield  $\text{Al}_2(\text{MoO}_4)_3$ .<sup>46</sup> Subsequently, La Forge<sup>47</sup> noted that a fluid, glassy phase was necessary for either reaction with or physically mixing with the sintering metal powders. Thus, mechanical interlocking enhanced adhesion by filling the voids in sintered metal coatings with the solidified glassy phase. Cole and Hynes<sup>48</sup> later showed that alumina ceramic-to-Mo-Mn metal seal strength varied with the alumina body purity, noting greater strengths in bodies with greater impurities. Cole and Sommer<sup>49</sup> subsequently postulated that the glass binder in the ceramic bodies was migrating into the sintering metal voids to promote adhesion. This became known as the "Glass Migration Theory", and Pincus's work was called the "Alumina Reaction Theory".

In performing studies on reactions between MnO/Mn and various oxides used in alumina ceramics, Denton and Rawson<sup>50</sup> showed compounds with  $\text{SiO}_2$ , MgO, CaO, and  $\text{Al}_2\text{O}_3$ . Their work tended to support Pincus's position. Floyd,<sup>42</sup> in working with Mo-Mn metallization and alumina ceramics with variable binder compositions, showed the importance of obtaining binder migration into the sintered metal layer. He also noted the formation of a modified spinel  $\text{Mn Al}_2\text{O}_4$ , by x-ray diffraction analysis. The location of the spinel could be varied, depending upon binder composition and firing conditions. Weaker bonds failed in the metal-ceramic interface region, where greater concentrations of the spinel were found. As mentioned earlier, larger alumina grain size resulted in greater adhesion strengths, but no explanation was offered. Floyd postulated that MnO decreased the viscosity of the Mg-Ca-Al-silicate glasses that were in the alumina ceramic body and thus promoted migration into the sintered metal.

The work of Reed and Huggins<sup>51</sup> tended to support the "Glass Migration Theory". The adhesion of metallizers composed of tungsten, molybdenum, and their respective oxides was poor on sapphire. When a  $\text{MnO}_2$ - $\text{TiO}_2$ - $\text{SiO}_2$  frit

was added to  $\text{MoO}_3$  and fired on sapphire, a vacuum-tight seal was formed. Electron probe microanalysis showed no diffusion of molybdenum into the ceramic. However, the original metallizer-ceramic interface regressed as  $\text{Al}_2\text{O}_3$  reacted with the  $\text{MnO}_2$ - $\text{TiO}_2$ - $\text{SiO}_2$  frit. Metallographic cross sections show a sintered spongy mass of molybdenum permeated with the resolidified frit.

When 99.5%  $\text{Al}_2\text{O}_3$  bodies were substituted for sapphire, the frit constituents diffused to a 60- $\mu\text{m}$  distance from the original interface via grain boundary migration. No metallizer metal, W or Mo, could be detected in the  $\text{Al}_2\text{O}_3$  grains or grain boundaries. A 94%  $\text{Al}_2\text{O}_3$  body showed even greater grain boundary penetration by the metallizer frit constituents. In this case, Mo was mixed with a  $\text{MnO}_2$ - $\text{TiO}_2$  frit. After firing, x-ray diffraction analysis revealed anorthite ( $\text{CaO} \cdot 2\text{SiO}_2 \cdot \text{Al}_2\text{O}_3$ ) crystals in the sintered metal sponge, in addition to the glassy phase which was normally found.

The work of Reed and Huggins raises many questions about the selection and composition of frit used in metallization systems. However, it does appear to support Pulfrich-Cole contentions that an intermediate oxide phase(s) must be present to react with the refractory metal and the ceramic. When taken in conjunction with Floyd's work,<sup>42</sup> which pointed toward deleterious compound formation ( $\text{MnAl}_2\text{O}_4$ ), it is seen that no simple mechanical interlocking model can be universally applied to metal-ceramic joints.

### C. SINTERING MODELS

Since so much of what has been reported with regard to metallizing ceramics is related to liquid phase sintering, it is necessary to describe the attempts at understanding this process. Recent reviews of the physics of sintering and liquid phase sintering in particular have been published by Kuczynski<sup>52</sup> and Eremenko et al.,<sup>53</sup> respectively. Both credit Kingery<sup>54,55</sup> with first effort in quantitatively treating this phenomenon. According to Kingery the driving force for densification is the negative hydrostatic pressure of pores in the liquid. Thus:

$$P_o = \frac{-2\gamma_{LV}}{r_p} \quad (1)$$

where  $\gamma_{LV}$  = liquid-vapor interfacial energy

$r_p$  = pore radius

Since,

$$\mu - \mu_o = RT \ln \frac{a}{a_o} = \Delta PV_o \quad (2)$$

The chemical potential or activity,  $a$ , can be expressed as

$$\ln \frac{a}{a_o} = \frac{K2\gamma_{LV}V_o}{r_p RT} \quad (3)$$

where  $K$  = constant relating the maximum contact area pressure to the overall hydrostatic pressure.

Therefore the reduction in free energy, which is the driving force and must take place for densification, occurs as the result of a decrease in liquid phase pore surface area.

It is generally recognized that densification of a sintering mass occurs in three stages, i.e., rearrangement, neck growth and coalescence. First, the formation of the liquid at elevated temperature permits rearrangement of the solid particles. Second, an increase in density occurs. One mechanism proposed in this stage includes the "solution-precipitation" process which depends upon the solubility of the solid in the liquid. Additional densification could also be simultaneously occurring by diffusion in or on the solid, viz, surface, grain boundary or volume diffusion processes. Finally, the slower stage or "coalescence process" is predominant and primarily involves surface, grain boundary and volume diffusion within the metal.

Kingery tested his proposed second stage solution-precipitation process with a liquid copper-solid iron sintering study. The rate-controlling process was by a diffusion of the dissolved iron in the liquid copper as opposed to a phase boundary reaction leading to solution of the iron.<sup>56</sup> The rate controlling equation was:

$$\frac{\Delta L}{L_o} = \left( \frac{K\delta D C_o \gamma_{LV} V_o}{RT r^4} \right)^{1/3} t^{1/3} \quad (4)$$

where K = constant depending on composition  
 $\delta$  = thickness of liquid between films  
 D = diffusion coefficient of solid in liquid  
 $C_o$  = solubility of solid in liquid  
 $\gamma_{LV}$  = liquid-vapor surface tension  
 $V_o$  = molar volume of dissolving liquid  
 r = solid particle radius  
 R = gas constant  
 T = absolute temperature  
 t = time

If in other systems the phase boundary reaction was rate-controlling, the correct relationship would be:

$$\frac{\Delta L}{L_o} = \left( \frac{K\gamma_{LV} C_o V_o}{RT} \right)^{1/2} r^{-1} t^{1/2} \quad (5)$$

Kuczynski<sup>52</sup> has pointed out that this model does not consider the large changes in particle size which occur during sintering. Furthermore, the small pores which are supposed to create the large hydrostatic pressures would collapse as larger ones formed. In addition, as applied to the metal-glass or metal-oxide systems of interest in the present study, the solubility of metals such as gold would be quite minimal, if at all existent.

However, there is some justification for pursuing its use. Cole<sup>57</sup> has compared the sintering of Ag-Pd compacts in the presence and absence of glass. In doing so, he essentially analyzed for sintering mechanisms, viz., grain boundary diffusion after Johnson and Cutler<sup>58</sup> or the solution-precipitation process of Kingery, for the glass-metal compacts. Johnson and Cutler have defined grain boundary diffusion in studying the shrinkage of powder compacts when spherical particles are assumed as follows:

$$\frac{\Delta L}{L_o} = \left( \frac{K\gamma a^3 D_B}{kTr^4} \right)^{0.31} t^{0.31} \quad (6)$$

where  $\Delta L/L_0$  = fractional shrinkage  
 K = numerical constant  
 $\gamma$  = surface free energy  
 a = lattice vacancy volume  
 $D_B$  = self-diffusion coefficient for  
           grain boundary diffusion  
 k = Boltzmann's constant  
 T = absolute temperature  
 r = particle radius  
 t = time

To compare the relative rates of shrinkage with and without glass present, Cole arranged the respective equations to plot L, compact powder diameter vs.  $t^n$ , where n varied between 0.31 and 1/3. This is best seen when equations (4) and (6) are rearranged to the form used by Cole:

$$L = L' - L' (K_0)^n t^n \quad (7)$$

where L = compact diameter at time t  
 L' = compact diameter at time t = 0  
 K<sub>0</sub> = constant for constant temperature T  
 n = 0.31 or 1/3 as required

The slope,  $L'(K_0)^n$ , would then produce a straight-line plot, if the Ag-Pd sintering fit the proposed mechanisms. The absolute value of the slopes would indicate which mechanism was rate-controlling. For the Ag-Pd without glass, Cole found that it did indeed fit the Johnson-Cutler grain boundary diffusion model. In addition, the activation energy for Ag was reasonably close to a previous value reported by Hoffman and Turnbull.<sup>59</sup>

When comparing the glass-free Ag-Pd samples with the glass-bearing Ag-Pd, Cole found the slopes of the glass-bearing samples were greater. He notes, however, that at low glass volume fractions, e.g., 4.5 percent, the slope was less than the glass-free samples. This implies that, at the sintering temperatures investigated, i.e., 600 to 750°C, the solution-precipitation mechanism is operative, when sufficient glass is present. Furthermore, the grain boundary mechanism as well might proceed at glass-free interfaces.

For his study, Cole employed a lead bismuth borosilicate glass, which is typically used in thick-film systems. He found Ag and Pd solubilities in the glass to be 0.49 and 0.13 wt pct, respectively. This raises questions pertaining to the variation of noble metal solubility in the various commercial metallizers and the impact it might have upon sintering kinetics, glass-metal wettability, and ultimately metallization properties, i.e., adhesion, conductivity, and bondability.

It will be necessary to undertake a more detailed study of gold-glass and gold-transition metal oxide systems with regard to these basic properties. Work similar to Cole's will be required for the gold systems in order to more clearly define its sintering habit. Additional tests would necessarily follow and include wetting studies viz., Kingery et al.,<sup>60-62</sup> and Pask and Fulrath<sup>63</sup>. The latter investigators have reported the change in contact angle in gold-sodium disilicate glass studies of 62° to 35° when measured in vacuo and in oxygen, respectively. Wetting and sintering information of this type will be helpful in formulating superior metallizers and in establishing improved process control parameters.

### III. PROGRESS OF THE CONTRACT STUDY

The first detailed study in the contract has been an evaluation of a broad range of gold thick-film inks (data on 17 are reported) and the adhesion they develop on alumina substrates of 96 and 99.5 wt pct purity purchased from two popular domestic vendors. The descriptions of these inks by their manufacturers, which were presented earlier,<sup>64</sup> have been included as Table 1. The study plan can be reviewed with reference to Fig. 1 which is schematic outline of the work.

#### A. CHEMICAL ANALYSES OF GOLD PASTES

An important part of the study has been the chemical analysis of the inks. Certain elements of the periodic series may receive further scrutiny in order to obtain more exact measures of their presence in particular inks, but the chemical analyses of gold inks are essentially complete. These are reported in Table 2.

The analytical methods used have been previously described.<sup>66</sup> The method of determination for each element reported in Table 2 may be deduced from the number of significant figures reported as explained below. Concentrations in three significant figures are reported for gold which was determined by wet chemistry. Two significant figures are reported for concentrations determined by atomic absorption spectroscopy. This technique was used where applicable to elements judged to have important functions in the ink or which were present in substantial quantities. A single significant figure is reported for concentrations of metals and oxides which were determined from the arithmetic means of optical emission spectrophotometry and solids mass spectrometry data. Where a question mark appears after these data, the result of optical emission spectrometry and solids mass spectrometry differed by a factor of 20 or more. The concentrations of the elements S, F, Cl, Br, P, and I were determined by mass spectrometry alone since those elements are not detected by emission spectrophotometry. The elements H, O, N, and C are not reported. Only elements which were detected in concentrations greater than 0.0005 wt pct were reported.

In all cases, detection was made of elements. Where concentrations are reported as oxides, these were determined by calculations using molecular weight ratios<sup>67</sup>. Where more than one oxide of a given metal was possible,

Table 1. Summary of Manufacturers' Data on Inks

<u>Ink</u>	<u>Type</u>	<u>Comments</u>	<u>Firing Conditions</u>	<u>Sheet Resistance</u>
A-1	Au; die and wire bonding. Micro-wave strip lines	99% + 0.5% Au in fired film. No burnishing. Glassless.	Range: 875°-980°C 5-6 min.	.001-.002 ohm/sq., .75 mil thick
A-2	Au; wire and die bonding	96% Au in fired film, Sn-Pb and Sn-Pb-Ag solders, no burnishing required, 800 psi adhesion.	Optimum: 800°-950°C, 5-6 min.	.003-.0035 ohm/sq., .5 mil thick
B-1	Au; die and wire bonding, high conductivity	5 mil lines with 7 mil spaces. Some leach resistance to Sn-Pb solder.	Range: 600-925°C 5-15 min. Optimum: 850°C.	.003 ohm/sq., .5 mil thick
B-2	Au; die and wire bonding, micro-wave	Fine line. 99% Au when fired. 5 mil lines. Glassless, high adhesion.	Range: 950°-1020°C 10 min. Optimum: 1000°C.	.003 ohm/sq., .5 mil thick
C-1	Au; die and wire bonding, micro-wave	High conductivity, almost all gold. High adhesion.	Range: 650°-1000°C.	.0018-.0022 ohm/sq., 1 mil thick
C-2	Au; die and wire bonding	5 mil lines, 5 mil spaces. Firable in air or in a reducing atmosphere.	Range: 900-950°C 10 min. 1050-1100°C (if Au melting is not a problem). Optimum: 850°C > 10 min.	.003-.005 ohm/sq., 1 mil thick
C-3	Au; die and wire bonding	4 mil lines, 4 mil spaces. Fine line, high conductivity.	Range: 875°-1000°C 10 min. Optimum: 900°-950°C.	.002-.006 ohm/sq., 1 mil thick
D-1	Au; die and wire bonding, high adhesion	92% Au when fired. Soldering not recommended with Sn-Pb solders.	Range: 815°-1010°C 5-15 min.	<.005 ohm/sq., 1 mil thick
D-2	Au; die and wire bonding, micro-wave	97-98% Au when fired	Range: 850-1000°C Optimum: 985°C 7-9 min.	.002 ohm/sq., 1 mil thick

Table 1. (Continued)

<u>Ink</u>	<u>Type</u>	<u>Comments</u>	<u>Firing Conditions</u>	<u>Sheet Resistance</u>
E-1	Au; die and wire bonding, beam-lead bonding	Fine line. 2 mil lines on 4 mil centers with metal mask. Slight leach resistance to Sn-Pb solders	Range: 850°-950°C Optimum: 900°C 5-10 min.	.003 ohm/sq., 1 mil thick
E-2	Au; die, wire, and beam-lead bonding	5 mil lines, 5 mil spaces. Fine line, high conductivity.	Range: 760°-950°C. Optimum: 850°C, 6-10 min.	.003 ohm/sq., .6 mil thick
F-1	Au; die and wire bonding	Dense fine-line prints.	Range: 730°-1000°C Optimum: 840°-950°C, 8-10 min.	.0032-.0036 ohm/sq., 1 mil thick
F-2	Au; die and wire bonding	Dense, fine-line prints, high conductivity.	Range: 730°-1000°C. Optimum: 840°-950°C, 8-10 min.	.0028-.0032 ohm/sq., 1 mil thick
F-3	Au; die and wire bonding, high conductivity	Dense, fine-line prints. Glassless, ~100% Au in fired film. Modest Sn-Pb solder leach resistance.	Range: 950°-1030°C. 1030°C.	.0013-.0017 ohm/sq., 1 mil thick
G-1	Au; die and wire bonding	3 mil lines, 3 mil spaces. Fine-line prints, high conductivity.	Range: 600°-1000°C Optimum: 950°C, 15 min.	.003 ohm/sq., .7 mil thick
G-2	Au; die and wire bonding	5 mil lines, 5 mil spaces Fine line.	Range: 850-1000°C. Optimum: 950°± 1°C, 15 min.	.003 ohm/sq., .6 mil thick
H-1	Au; wire, die, and beam-lead bonding	Fine line, glass-free, high conductivity. Peel strength 2 to 3 times greater than fluxed gold. Thermal conductivity high. High compatibility with most resistor and multilayer dielectrics.	Optimum: 980°-1020°C, 5-15 min. at peak.	.003 ohm/sq., .5 mil thick



Table 2. Chemical Analyses of 17 Gold Conductor Inks  
(Proportions shown in wt pct of inorganic solids.)

NOBLE METAL	INKS	A-1	A-2	B-1	B-2	C-1	C-2	C-3
Ag		.03	.03	.05	.05	.03	.03	.03
Au		99.5	94.8	97.6	97.9	96.4	99.6	92.2
Pd		.002	.002	.01	.007			.008
Pt		.02	.002					
Ru								.002
Rh								
Hg								
<u>CLASS-ACTIVE METAL OXIDES</u>	<u>FUNCTION CODE<sup>65</sup></u>							
Al <sub>2</sub> O <sub>3</sub>	I,F	.04	0.11	0.039	.006	.08	0.13	.17
As <sub>2</sub> O <sub>3</sub>	F*	.003	.001					
B <sub>2</sub> O <sub>3</sub>	F	1.	.2	.3		.50	1.	.3
BaO	M	0.062	.01			.01	1.5	.06?
CaO	M	.001	.001	.004	.07?	.003	.03	.7
CdO	M,I				.39			1.3
Cs <sub>2</sub> O	M							
K <sub>2</sub> O	M	.067	.008			.002	.01	.04?
MgO	M	.003		.003	.002	.003		.03
Na <sub>2</sub> O	M	.04	.008	.004	.007	.004	.03	.01
PbO	M,I	.1	4.4	2.3	.003	2.5	.05	2.1
Rb <sub>2</sub> O	M,I	.002						
SiO <sub>2</sub>	F	.9	.4	.1	.06	.2	1.	1.
SnO <sub>2</sub>	M					.001		.008
SrO	M	.005	.002				.032	.005
TiO <sub>2</sub>	I	.007	.08	.01	.005	.007	.05	.05
Y <sub>2</sub> O <sub>3</sub>	M							
ZnO	M,I		.01	.002	.002	1.	.02	0.017
ZrO <sub>2</sub>	I,F	.007		.001		.4?	.08?	.01
P <sub>2</sub> O <sub>5</sub>	F					.01		.1
<u>OTHER METAL OXIDES</u>								
Bi <sub>2</sub> O <sub>3</sub>		.6?		.002	1.0	.002	.01	2.0
Co <sub>3</sub> O <sub>4</sub>								
Cr <sub>2</sub> O <sub>3</sub>		.001	.001			.001		
CuO		.8	.005	.005	.59	.5	.003	.01
Fe <sub>3</sub> O <sub>4</sub>		.009	.006		.004	.002	.004	.003
NiO		.003	.001					
WO <sub>3</sub>								
Sb <sub>2</sub> O <sub>3</sub>		.8						.005
<u>ANIONS</u>								
Cl		.005	.01		.001	.004	.007	.01
F		.001						
I		.1	.2					
S		.001	.002	.002				
Br								.001

Table 2. Continued.

NOBLE METAL	D-1	D-2	E-1	E-2	F-1	F-2	F-3	G-1	G-2	H-1
Ag	.03	.06	.2	.06	.06	.03	.03	.06	.05	.02
Au	95.7	95.8	93.2	91.8	86.4	90.7	98.8	95.0	97.8	98.3
Pd	.002		.006	.04	.03		.002	.007	.002	.02?
Pt									.002	
Ru		.002								
Rh	.02									
Hg				.004?						
<u>GLASS-ACTIVE METAL OXIDES</u>										
Al <sub>2</sub> O <sub>3</sub>	.002	.004	.08	.1	.04	.08	.004	.006	.013	
As <sub>2</sub> O <sub>3</sub>										
B <sub>2</sub> O <sub>3</sub>			.6	.2	1.	1.		.6	1.	
BaO			.02?	.006	.004	.007		.03	2.4	
CaO			.01	.007	.003	.003			.006	
CdO	3.	.93	.005	.002	.002			.060	.01?	.23
Ca <sub>2</sub> O									.001	
K <sub>2</sub> O			.08	.02					.1	
MgO			.003	.005					.003	
Na <sub>2</sub> O					.003	.007	.03	.01	.07?	.004
PbO	.004	.001	2.5		.76	.64	.005	2.8	1.0	.002
Rb <sub>2</sub> O									.003	
SiO <sub>2</sub>	.4	.04	2.	.6	.9	.9	.04	.4	.9	.06
SnO <sub>2</sub>	.008	.002	.002	.002						.004
SrO			.001			.004	.002	.002	.008	.002
TiO <sub>2</sub>	.003	.003	.07	.007			.005	.1	.03	.003
Y <sub>2</sub> O <sub>3</sub>					.001	.001				
ZnO			.007	.004	.002	.002	.004	.02	.005	
ZrO <sub>2</sub>			.03		.47	.57	.001	.05	.003	
P <sub>2</sub> O <sub>5</sub>				.1						
<u>OTHER METAL OXIDES</u>										
Bi <sub>2</sub> O <sub>3</sub>	4.9	2.0	3.0	5.6	10.4	7.4	.003	.003	.003	
Co <sub>3</sub> O <sub>4</sub>					.03				.04	
Cr <sub>2</sub> O <sub>3</sub>	.03	.008	.009	.009	.004	.003	.001		.003	.001
CuO	.001	.25	.03	.008	.005	.003	.75		.003	.88
Fe <sub>3</sub> O <sub>4</sub>			.03	.09	.03?	.003		.1	.03	
NiO			.005	.004	.005		.001			
WO <sub>3</sub>					4.	4.				
Sb <sub>2</sub> O <sub>3</sub>										
<u>ANIONS</u>										
Cl	.04	.009	.14	.02	.004	.02	.002	.02	.02	.002
F			.002						.001	
I										
S	.1	.04	.03	.03	.002	.002	.001	.003	.001	
Br										

the one selected was the one with the highest negative free energy of formation per mole of the element at a temperature of 1300°K which was arbitrarily chosen to approximate the firing temperature. In most cases the oxide most stable at 1300°K is also the commonly available one. Some elements are doubtless introduced to the inks as carbonates (which give up CO<sub>2</sub> on firing to become oxides) or as other oxides than the ones we calculated. This could, in part, account for the discrepancies between 100 pct and the sum of the constituent weight fractions we reported for each ink in Table 2. A more important reason for the discrepancies is that both solids mass spectrometry and emission spectrometry are only semiquantitative methods of analysis. I.e., without careful standardization, they have error factors of ~3.<sup>66</sup>

As previously noted,<sup>64</sup> the analyses were performed on samples baked on oxygen at 350°C or 450°C, and each of the concentrations reported is expressed as a weight percent of the total inorganic solids. This format allows the straightforward blending of inks similar to those analyzed.

If one assumes certain rationalizing criteria, it will greatly simplify the interpretation of Table 2. The assumptions we used are listed below. Their use is particularly helpful in studying the ink constituents which have functional importance in the fired conductor film.

1. Ink manufacturers may make or buy several-component glasses which they modify and mix. The glasses are often made with technical grade or even more impure starting materials. Hence, the inks can contain a large number of traces of elements for which no functional use can be ascribed.
2. Inks are blended on mixing plates, on three-roll paint mills, and with other equipment. Traces of materials such as Ru, Pd, Rh, Pt, and Ir are probably introduced to gold conductors through less-than-thorough cleaning of such mixing equipment. (The elements named are used in thick-film composition for making resistors and other conductor types.)
3. The elements sodium and potassium are probably accidental additions, since they are considered extremely detrimental to the properties of insulating (crossover and capacitor) dielectrics.

4. Silver is probably introduced as an impurity in the gold powder. As with small amounts of other precious metals, the silver is believed to dissolve in the gold with no harmful effects.
5. Sulphur, bromine, iodine, chlorine, fluorine, and carbon should be largely volatilized from or burned out of the inks by firing them in air between  $\sim 500$  and  $1000^{\circ}\text{C}$ . Their presence has been noted in order to provide clues to the process origins of the gold powders, the glass constituencies, etc.
6. The substantive presence of copper oxide is the key to whether any reactive bonding has been sought by the formulator of the ink. The presence of cadmium indicates that substantial adhesion can be attained at moderate firing temperatures ( $1000^{\circ}\text{C}$ ) without the presence of significant amounts of other materials.
7. For each ink, if one notes the amount of gold present in the ink and further notes the relative proportion of the principal remaining functional constituents of the inks, Table 2 can be greatly simplified.

Using considerations from earlier work<sup>69,70,71,72</sup> a first order classification of the inks can be made on the basis of their probable adhesion mechanism(s). The simplified analytical data and groupings are presented in Table 3.

## B. ADHESION AND CONDUCTIVITY MEASUREMENTS

### 1. Sample Preparation

The second major area of work performed this quarter on the study shown in Fig. 1 was the physical evaluation of inks, including the fabrication of test substrates and the measurement of adhesion. Tests were performed on substrates which passed certain criteria. Substandard substrates, revealed to be poor by visual inspection or by printer vacuum hold-down, were discarded. In normal practice, 10 to 15 percent of some lots of 96 wt pct substrates must be rejected, but all of the lots used in this study gave better yields.

The adhesion test chosen for this part of the contract study was the strip peel test used with success in earlier work.<sup>71</sup> The test pattern

Table 3. Simplification of the Chemical Analysis Data for Thick-Film Gold Conductors Grouped by Binder Type

Inks containing no appreciable amount of copper			
Ink	Au (wt pct)	Total Binder wt pct	Binder Constituents
A-2	94.8	5	4/5 PbO; also SiO <sub>2</sub> , B <sub>2</sub> O <sub>3</sub> , and Al <sub>2</sub> O <sub>3</sub>
B-1	97.7	3	4/5 PbO; also B <sub>2</sub> O <sub>3</sub> , SiO <sub>2</sub> , and Al <sub>2</sub> O <sub>3</sub>
C-2	99.6	4*	BaO, SiO <sub>2</sub> , and B <sub>2</sub> O <sub>3</sub> ~1:1:1; also Al <sub>2</sub> O <sub>3</sub>
C-3	92.2	8	Bi <sub>2</sub> O <sub>3</sub> , PbO each 1/4; also CdO, SiO <sub>2</sub> , and CaO
D-1	95.7	8*	5/8 Bi <sub>2</sub> O <sub>3</sub> , 3/8 CdO; also SiO <sub>2</sub>
E-1	93.2	8	Bi <sub>2</sub> O <sub>3</sub> , PbO, and SiO <sub>2</sub> ~1:1:1, also B <sub>2</sub> O <sub>3</sub>
E-2	91.8	7	4/5 Bi <sub>2</sub> O <sub>3</sub> ; also SiO <sub>2</sub> , B <sub>2</sub> O <sub>3</sub> , Al <sub>2</sub> O <sub>3</sub> , P <sub>2</sub> O <sub>5</sub>
F-1	86.4	17	1/2 Bi <sub>2</sub> O <sub>3</sub> ; also WO <sub>3</sub> , B <sub>2</sub> O <sub>3</sub> , SiO <sub>2</sub> , PbO, ZrO <sub>2</sub>
F-2	90.7	15	1/2 Bi <sub>2</sub> O <sub>3</sub> ; also WO <sub>3</sub> , B <sub>2</sub> O <sub>3</sub> , SiO <sub>2</sub> , PbO, ZrO <sub>2</sub>
G-1	95	4	5/8 PbO; also B <sub>2</sub> O <sub>3</sub> , SiO <sub>2</sub>
G-2	97.8	6	2/5 BaO; PbO, B <sub>2</sub> O <sub>3</sub> , SiO <sub>2</sub> ~1:1:1
Inks containing substantial copper			
A-1	99.5	4*	CuO, Sb <sub>2</sub> O <sub>3</sub> , SiO <sub>2</sub> , B <sub>2</sub> O <sub>3</sub> , and Bi <sub>2</sub> O <sub>3</sub> ? ~1:1:1:1:1
B-2	98	2	1/2 Bi <sub>2</sub> O <sub>3</sub> ; remainder CuO and CdO 3:2
C-1	96.4	5	1/2 PbO; also ZnO, CuO, B <sub>2</sub> O <sub>3</sub> , ZrO <sub>2</sub> ?, and SiO <sub>2</sub>
D-2	95.8	3	2/3 Bi <sub>2</sub> O <sub>3</sub> ; remainder CuO and CdO 1:4
F-3	98.8	1	CuO
H-1	98.3	1	CuO, CdO ~4:1

Notes: Binder constituents listed in decreasing order of wt. fractions according to Table 2.

\* Denotes a substantial discrepancy between 100 pct and the sum of the binder and gold wt pcts.

? Indicates an uncertainty in Table 2 as explained in the text.

of Fig. 2(a) was designed to permit the simultaneous bonding of five 0.040 in.-wide x 0.002 in.-thick strips of a gold foil lead frame shown in Fig. 2(b) to the five 0.020 in.-wide conductor lands on the test substrate. The test pattern of Fig. 2(a) also contains five-line resolution patterns with 0.005, 0.0025, 0.0075, and 0.00375 in. lines and spaces lying both parallel and perpendicular to the squeegee travel direction; a 100-square Kelvin connection conductivity test pattern; and square and strip test patterns for possible solder or polymer cement adhesion testing.

Fabrication of the adhesion test parts was done in keeping with standard practice. Table 4 describes the printing characteristics of the 17 inks and their resolution capabilities. A series of four flat-topped furnace profiles were established for the BTU furnace for peak temperatures of 850<sup>o</sup>, 900<sup>o</sup>, 950<sup>o</sup>, and 1000<sup>o</sup>C. If a belt speed of 3 in. per minute is used, these profiles hold a part for 10 minutes at the peak furnace temperature. The profiles shown in Fig. 3 are tracings of the recorder charts from actual profiles determined using a chromel-alumel thermocouple.

Settling, drying, and firing data for the printed test patterns are shown in Table 5. In Appendix A, additional details are given concerning the printing, drying, and firing processes and the methods developed for fabrication of the gold lead frames.

As shown in Fig. 1, parts made with each combination of conductor ink and substrate were prepared with two series of firings: (1) the closest approximation of our firing profiles to the manufacturers' suggested firing for the conductor (see Table 1) and (2) the firing described in (1) above, followed by two dielectric firings and three resistor firings. The furnace profiles chosen (850<sup>o</sup>, 900<sup>o</sup>, 950<sup>o</sup>, or 1000<sup>o</sup>C flat-topped) for the refirings simulate the firings of thick-film resistor and dielectric systems which are compatible with each conductor.

Adhesion and sheet resistance data have been taken on samples from most of the points of a matrix of the 17 inks x 4 substrates x 2 firing sequences. On the basis of chemical analyses, the manufacturers' data, and our experience, it was judged that certain inks warranted still other specific firings. Samples were prepared accordingly.

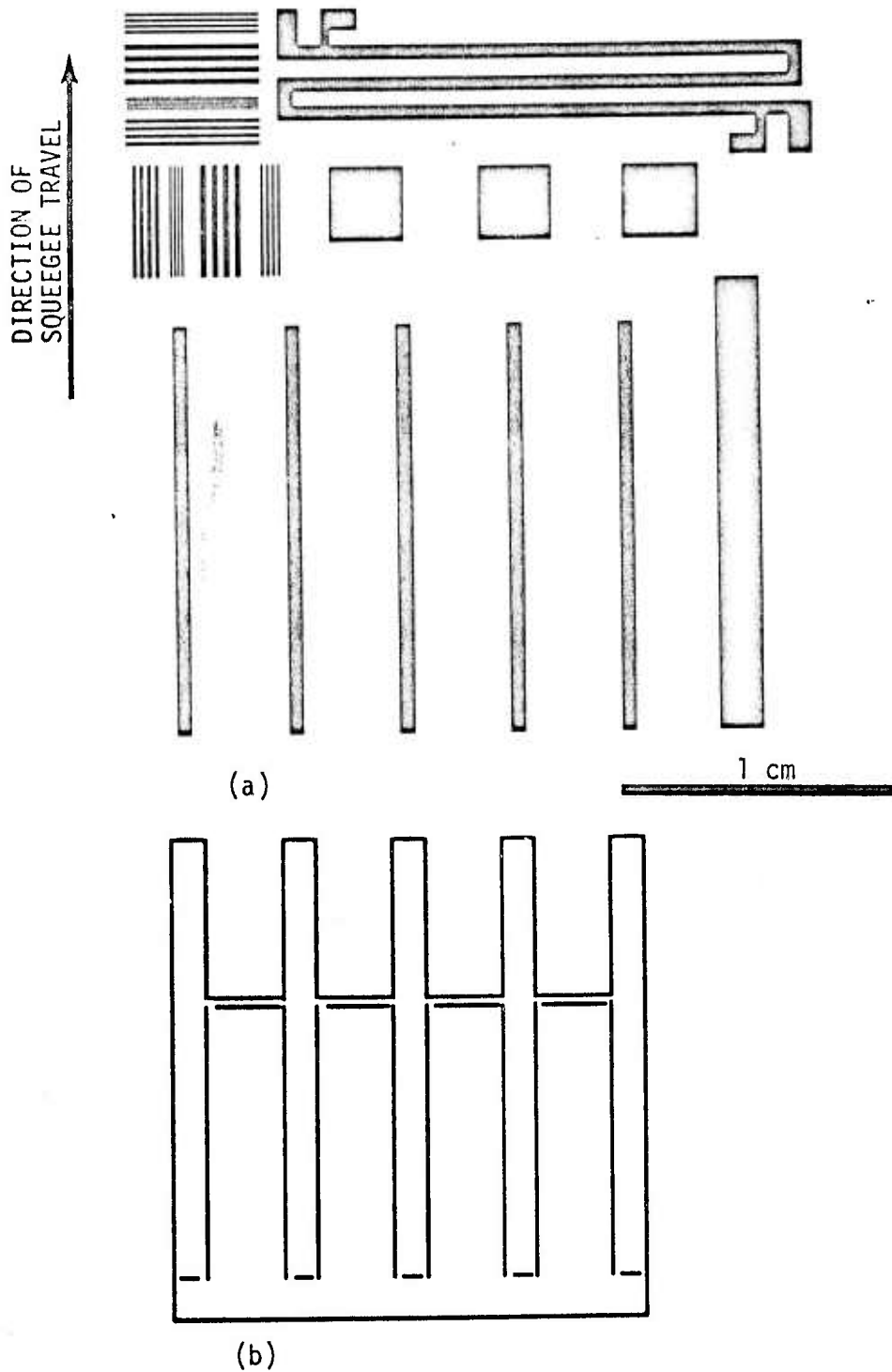


Figure 2. (a) Conductor test pattern, (b) frame to match conductor pattern in (a).

Table 4. Notes on the Printing Characteristics of Gold Thick Film

Ink Code	As-Received Consistency (rest viscosity)	Resolution of 2.5, 3.75, 5.0 and 7.5 mil lines and spaces after firing				Other Notes	
		90 wt. pct. Al <sub>2</sub> O <sub>3</sub>		99.5 wt. pct. Al <sub>2</sub> O <sub>3</sub>			
		Substrate A	Substrate C	Substrate B	Substrate D		
A-1	(too low)	A.R.	A.R.	A.R.	A.R.		
A-2	medium	7.5 O.K. R.R.	7.5 O.K. R.R.	5.0, 7.5 O.K. R.R.	7.5 O.K. R.R.		
B-1	(too low)	7.5 O.K. R.R.	7.5 O.K. R.R.	A.R.	A.R.		
B-2	required thinning	5.0, 7.5 O.K. R.R. and D.P.	5.0, 7.5 O.K. R.R. and D.P.	All O.K.	All O.K.		
C-1	good (medium)	5.0, 7.5 O.K. R.R.	All O.K.	5.0, 7.5 O.K. R.R.	All O.K.		
C-2	(medium-high)	A.R.	A.R.	A.R.	7.5 O.K., R.R.		
C-3	(medium)	2.5, 3.75 D.P. Rest O.K.	2.5 D.P. Rest O.K.	2.5 D.P. Rest O.K.	2.5, 3.75 D.P. Rest O.K.		
D-1	(medium)	7.5 O.K. R.R.	7.5 O.K. R.R.	5.0, 7.5 O.K. R.R.	7.5 O.K. R.R.		
D-2	(high)	2.5 D.P. Rest O.K.	2.5, 3.75 D.P. Rest O.K.	All O.K.	2.5 D.P. and run, rest O.K.	This ink dries rapidly on the screen if the printing temperature rises much above 68-72°F. Ambient humidity may also have influence at higher temperatures.	
E-1	(high)	7.5 O.K. R.R.	A.R.	7.5 O.K. R.R.	7.5 O.K. R.R.		
E-2	(high) R.T.	2.5 D.P. Rest O.K.	2.5 D.P. Rest O.K.	2.5 D.P. Rest O.K.	2.5 D.P. Rest O.K.		
F-1	(very high) M.S.T.	2.5, 3.75 D.P. Rest O.K.	2.5, 3.75 D.P. Rest O.K.	2.5, 3.75 D.P. Rest O.K.	2.5, 3.75 D.P. Rest O.K.		
F-2	(very high) M.S.T., R.T.	7.5 O.K. R.R.	A.R.	7.5 O.K. R.R.	5.0, 7.5 O.K. R.R.		
F-3	(very high) M.S.T.	7.5 O.K. Rest D.P.	7.5 O.K. Rest D.P.	7.5 O.K. Rest D.P.	5.0, 7.5 O.K. Rest D.P.		
G-1	(medium) R.T.	7.5 O.K. R.R.	A.R.	A.R.	7.5 O.K. R.R.		Ink stringy, dry printed before thinning.
G-2	(medium) R.T.	7.5 O.K. R.R.	7.5 O.K. R.R.	7.5 O.K. R.R.	7.5 O.K. R.R.		Ink stringy, dry printed before thinning.
H-1	(medium) R.T.	7.5 O.K. R.R.	7.5 O.K. R.R.	7.5 O.K. R.R.	7.5 O.K. R.R.		Tended to dry on screen.

Abbreviations:

- M.S.T. - marked ahead thinning
- R.T. - required thinning
- D.P. - ink failed to transfer to substrate resulting in gaps in printed pattern (dry print)
- R.R. - rest of lines run together
- A.R. - all run (ink transferred but no lines resolved)

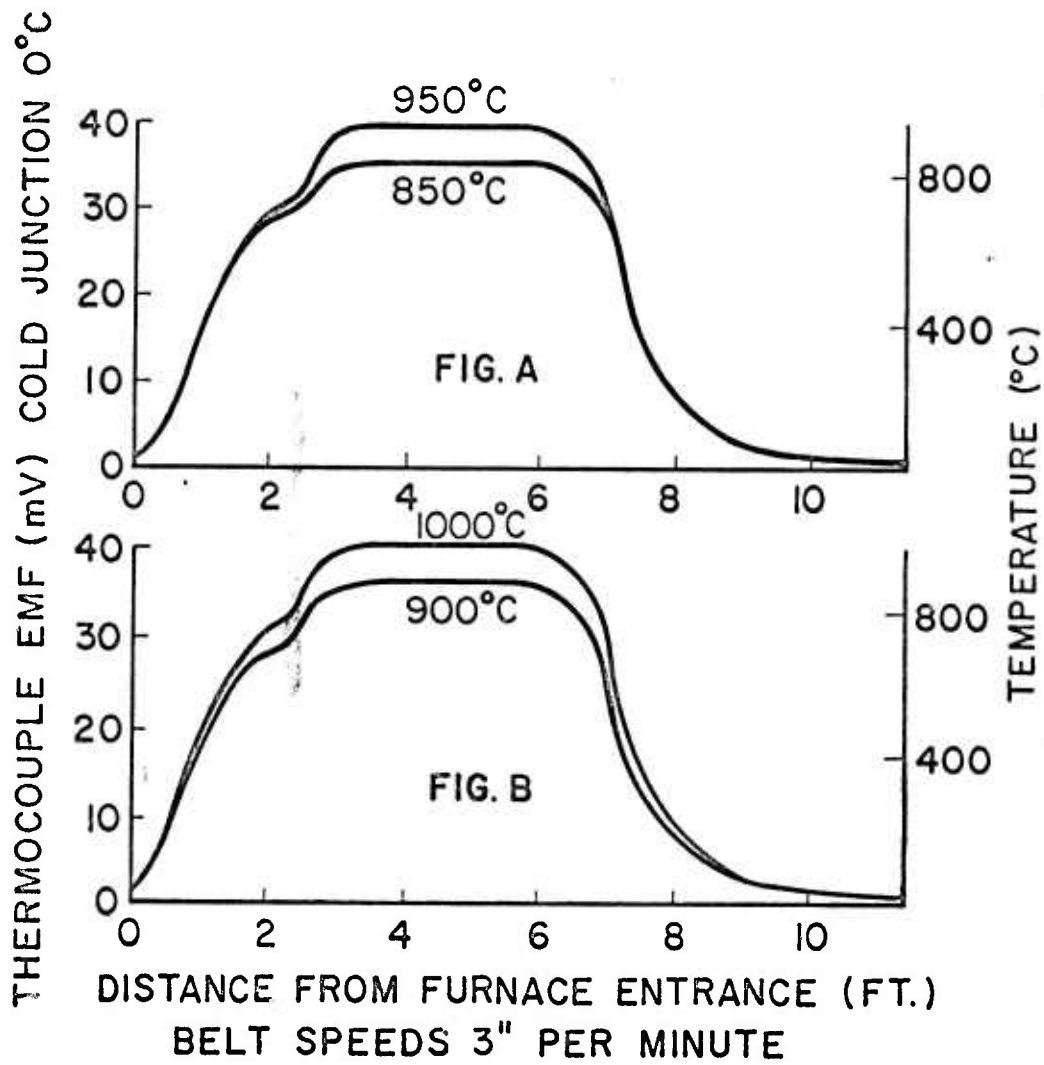


Figure 3. Belt furnace temperature profiles used in the study.

Table 5. Gold Thick-Film Drying and Firing Process Parameters

Ink Code	*Drying Time and Temperature	Conductor - First Firing		Refiring			
		Peak Firing Temp., °C	Belt Speed	Crossover Dielectric Simulation		Resistor Simulation	
				Peak Temp., °C	Belt Speed	Peak Temp., °C	Belt Speed
A1	15 minutes at 150°C	1000°/3" min.		850°/3" min.		900°/3" min.	
A2	15 minutes at 150°C	900°/3" min.		850°/3" min.		900°/3" min.	
B1	15 minutes at 125°C	850°/3" min.		850°/3" min.		900°/3" min.	
B2	15 minutes at 125°C	1000°/3" min.		850°/3" min.		900°/3" min.	
C1	15 minutes at 125°C	850°/3" min. 1000°/3" min.		900°/3" min. 900°/3" min.		1000°/3" min. 1000°/3" min.	
C2	15 minutes at 125°C	950°/3" min. 950°H <sub>2</sub> /10 min. soak		900°/3" min. not refired		1000°/3" min. not refired	
C3	15 minutes at 125°C	900°/3" min.		900°/3" min.		1000°/3" min.	
D1	15 minutes at 150°C	850°/3" min.		900°/3" min.		1000°/3" min.	
D2	15 minutes at 150°C	900°/3" min. 1000°/3" min.		900°/3" min. 900°/3" min.		1000°/3" min. 1000°/3" min.	
E1	15 minutes at 125°C	900°/3" min.		900°/3" min.		850°/3" min.	
E2	15 minutes at 125°C	850°/3" min.		900°/3" min.		850°/3" min.	
F1	15 minutes at 125°C	900°/3" min.		900°/3" min.		850°/3" min.	
F2	15 minutes at 125°C	900°/3" min.		900°/3" min.		850°/3" min.	
F3	15 minutes at 125°C	1000°/3" min.		900°/3" min.		850°/3" min.	
G1	15 minutes at 125°C	850°/3" min.		950°/3" min.		850°/3" min.	
G2	15 minutes at 125°C	950°/3" min.		950°/3" min.		850°/3" min.	
H1	15 minutes at 150°C	1000°/6" min.		900°/3" min.		850°/3" min.	

\* After a minimum of 15 minutes at room temperature.

Bonding of the lead frame, shown in Fig. 2(b), to the test pattern was done at the substrate edge end of the five 0.020 in.-wide line conductor lands. A Jade Corporation (Huntingdon Valley, Pa.) Mark 1 MTP bonder was used to make the thermocompression adhesion test bonds. A 2 in.-long thermode with a 0.2 in.-wide flat face for the length of the thermode apex was selected. The flat thermode bonding face was allowed to overlap the conductor land ends by  $\sim 0.075$  in., while the lead frame overlapped the land ends by  $\sim 0.175$  in. to produce the final geometry shown in Fig. 4(a). A thermode temperature of  $500^{\circ}\text{C}$  and a dwell time of 1 second were used. A ram force of  $\sim 300$  lbs. is developed by the 6-psi ram drive pressure setting used. A Jade compliant base supported the substrate under the ends of the 0.020 in.-wide conductor lands with 0.046 in.-diameter pins. These pins were in turn supported by individual cantilever beams. Despite the precautions taken to compensate for substrate camber, a substantial number of "C" substrates broke in bonding, and thus required the bonding of other parts. Very few of the other substrates, A, B, or D, broke in bonding.

## 2. Experimental Procedures

Conductivity test patterns were inspected with an Olympus SZ Stereo Microscope at 8X. The resistance of the 100 square pattern was measured using four-point (Kelvin) contacts made with a Wentworth Laboratories, Inc., (Brookfield, Conn.) Model MP-02 Probe Station and a Non-Linear Systems, Inc. (Del Mar, California) X-2 Digital Voltmeter. The data reported are simply the total resistance measured for each sample divided by 100 squares.

Adhesion testing was performed at 0.5 in. per minute with the apparatus and in the manner previously described.<sup>71</sup> For samples which peeled, the peel stress reported is two times the peel load measured, since the tested conductor lands are 0.5 mm (0.020 in.) wide. It should be noted that data so calculated will indicate too high an adhesion strength for inks that did not hold definition, i.e., those which spread to a greater width than 0.5 mm. When the measurements of peeled strip widths are complete, these data can be refined accordingly.

Thick-film paste solids were prepared for scanning electron microscope studies from the conductor pastes, using the techniques described above for preparing the materials for chemical analysis. Oxygen baking at  $350^{\circ}\text{C}$

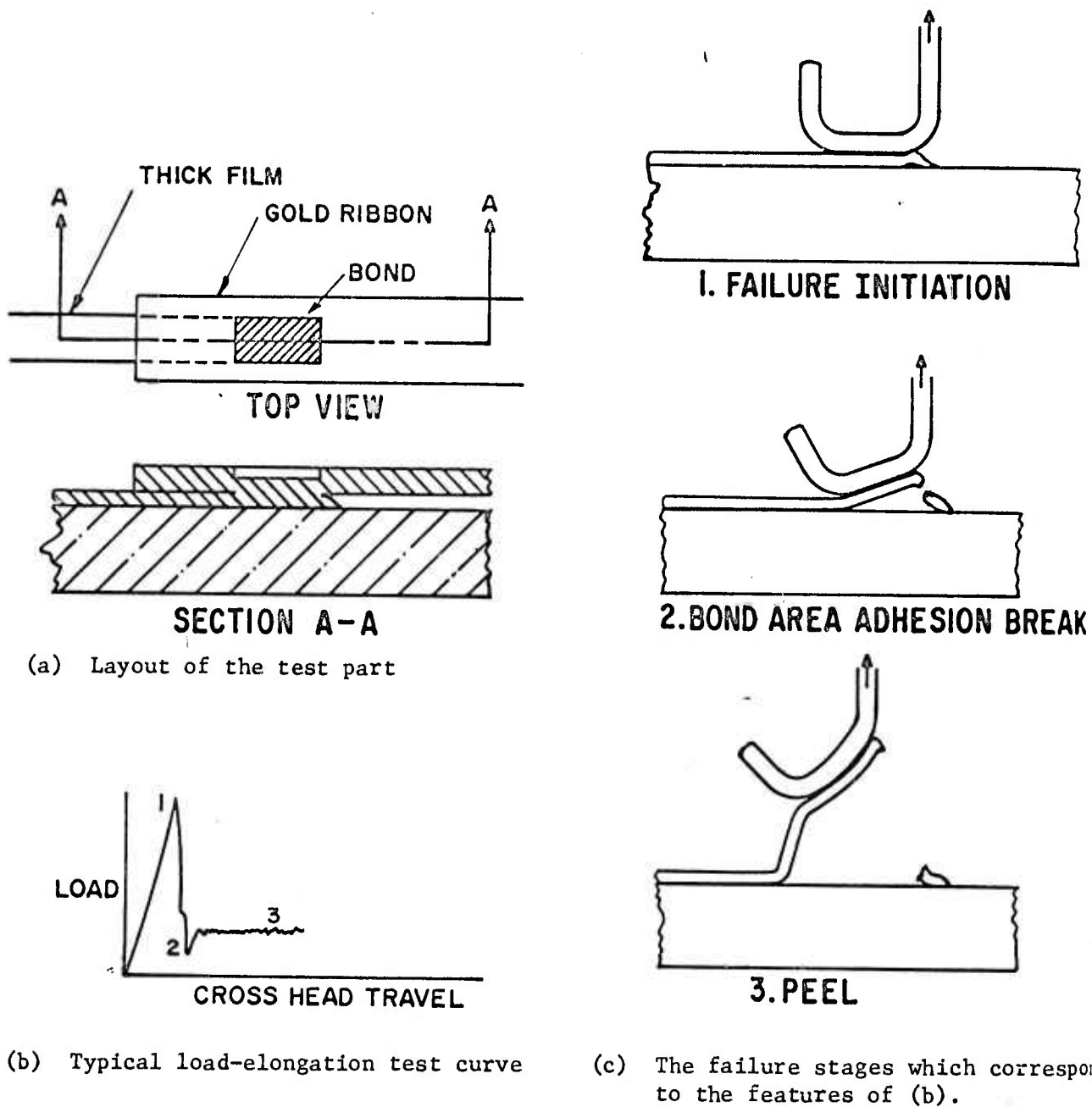


Figure 4. The RCA peel test (nominally after Ref. 71).

produced no apparent sintering in the paste solids. Two methods were used to mount the samples for study in the SEM.

Method 1. Silver paste was used to coat a sample holder. Dried ink solids crumbled by pressing between sheets of glassine weighing paper were sprinkled onto the still tacky sample holder. The powder not held by silver paste was removed by turning the sample holder upside down after the silver paste had been allowed to dry.

Method 2. Lumps of the dried ink solids were made to adhere to sample mounting stems with the silver paste, and silver paste stripes were painted over portions of the surface to reduce surface charging which can occur because of the poor gold particle-to-gold particle conductivity.

Samples prepared by both methods above were further prevented from surface charging by an evaporated coating of  $\sim 100 \text{ \AA}$  of gold.

### 3. Results

Conductivity data are shown for the 17 inks, singly and multiply fired, in Fig. 5(a), (b), and (c). The format of the figures requires some explanation, but it allows the data to be consolidated. The reader should note that the data from singly fired samples are on the left and from multiply refired samples on the right. He should further note that data from the 96 wt pct alumina, A and C, have been grouped together as have those of the 99.5 wt pct aluminas, B and D. The data have been grouped for graphical presentation by ink type and by frit content.

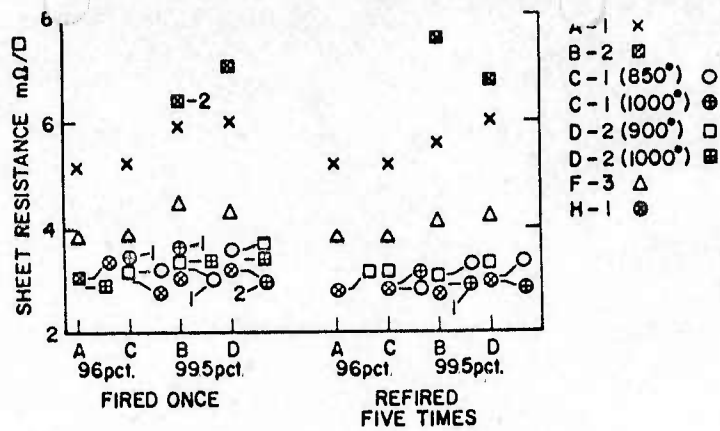
Figure 5(a) shows the results of inks which contain copper oxide and are, therefore, classified as either reactively bonded\* or mixed bonded\*\* conductors.

Most of the points represent the average sheet resistance of three samples. Where numbers are associated with the points, as in the other parts of Fig. 5, irregular prints prevented good measurements on all three conductivity patterns. The number states the total data points (if other

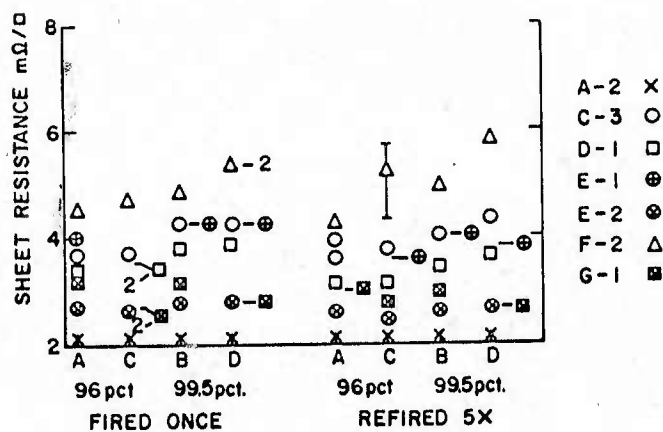
---

\* "Reactively bonded" and "frit-bonded" are defined in Ref. 72.

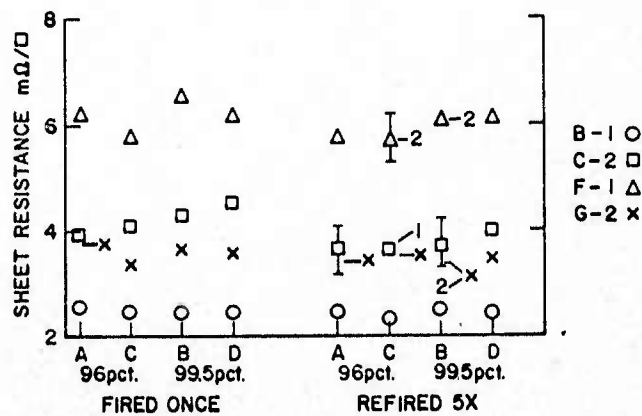
\*\*Mixed bonded inks are defined here as those which may bond by frit-bonding and/or reactively bonding.



(a)



(b)



(c)

Figure 5. Sheet resistance for 17 inks: (a) reactively and mixed-bonded gold inks, (b) frit-bonded inks containing 90 to 97 wt pct gold, and (c) other frit-bonded inks.

than three) which were considered to be reliable, on the basis of visual inspection and resistance measurement, and which were averaged to give the value reported. Where no data point is shown for a group, the conductivity pattern had printed too poorly for the data to be meaningful. Scatter bands, showing minimum and maximum values of the data, were drawn only when the data used spread more than 10 percent from the arithmetic mean. For much of the data, scatter was less than 5 percent of the mean.

Where plotting the data directly on the graph would cause data points to overlap, some of the data have been shifted to the right. The horizontal portion of the leader indicates where the point would otherwise fall.

The second group of inks is the frit-bonded class containing between 90 and 97 wt pct gold. Frit-bonded inks with less than 3 wt pct frit are projected to have too little adhesion strength for general use. Those with more than 10 wt pct are judged to be overloaded with frit. Interestingly, the lowest sheet resistance ink of all groups was not a reactively bonded fritless ink, but was a conventionally frit-bonded ink, A-2 (see Fig. 5 (b)). The resistance of others in the frit-bonded class ranged nearly to  $6 \text{ m}\Omega/\text{sq.}$ , with most demonstrating  $\sim 3$  to  $4 \text{ m}\Omega/\text{sq.}$  As with the reactively bonded inks of Fig. 5(a), sheet resistance was generally independent of substrate purity and was reduced only a few percent, if at all, by multiple firing.

As might be expected, the inks which were relegated to Fig. 5(c) have a broad spectrum of sheet resistances which reflect their glass constituency. The highest and one of the lowest sheet resistances occurred in this group.

#### C. ADHESION TESTS

In Table 6 the adhesion data have been grouped to give indications of failure modes, the number of data used, the arithmetic mean loads, and their coefficient of variation. In testing, the three bonds which appeared best were tested on each of the two substrates per matrix point.

In running the tests, we encountered several failure modes for the adhesion test. These were noted from the Instron recorder test chart and from the appearance of the test sample during and after testing. The several modes can be understood with reference to Fig. 4 taken from our earlier study.<sup>71</sup> The most desirable failure mode from the point of view

Table 6. Field Adhesion Test Data

Ink	Fired	A			B			C			D						
		N	Mode	Ratio	X	%	N	Mode	Ratio	X	%	N	Mode	Ratio	X	%	
A-1	once	6 a		3.1	35.												
	refired 5x	6 a		16.5	65.	6 a		26.8	92.	6 a		5.6	46.	5 a		3.6	17.
A-2	once	6 e/b peel	2	24.6	7.1	6 b		17.6	5.1	4 c/b peel	3	26.4	7.6	6 b		16.3	9.5
	refired 5x	3 e 5 b	peak 11.	27.7 20.2	17. 11.	6 b 6 b		15.9	7.2	3 e 5 b	peak 6	26.9 23.6	41. 10.8	6 b 6 b		14.6	15.
B-1	once	6 b		14.4	9.2	6 b		14.0	4.7	4 b		14.4	4.1	6 b		10.2	11.
	refired 5x	6 b		9.5	8.0	6 b		9.84	8.0	6 b		9.36	6.8	6 b		9.54	5.4
B-2	once	5 e 5 e	peak peel	53.2 19.6	17. 16.	6 a		86.6	14.	6 a		65.4	16.	6 a		55.2	11.
	refired 5x	5 a		46.2	19.	6 a/e 2 peak		78.3	13.	6 a		57.8	7.2	5 a		49.0	12.
C-1 850	once	6 a		50.4	1.1	6 a		42.8	45.	6 a		84.3	25.	3 b/e		19.9	1.2
	refired 5x	6 b		14.3	8.9	6 b		8.70	8.32	6 b		14.8	9.2	6 b	peel	5.8	26.
C-1 1000	once	4 b		25.2	7.6	6 b		10.2	6.9	6 b		22.4	1.0	5 b		8.0	16.
	refired 5x	6 b		14.0	6.1	6 b		7.8	7.8	6 b		14.0	3.8	5 b		7.8	12.

Table 6. Continued.

Ink	Fired	A			B			C			D				
		N	Mode	Ratio	X̄	V %	N	Mode	Ratio	X̄	V %	N	Mode	Ratio	X̄
C-2	once	5	a	6.36	12.	18.9	70.	6	a	6.03	25.	6	a	6.28	32.
	refired 5x	5	b	6.00	11.	5.36	8.6	5	b	6.64	3.9	5	b	5.72	7.7
C-3	once	5	b	8.84	3.4	7.56	14.0	3	e/b	2	1.1	6	b	7.84	6.9
	refired 5x	6	b	9.16	7.0	8.50	7.7	6	b	9.66	6.1	5	b/d	4	7.88
D-1	once	4	d	16.8	9.5	13.6	17.	4	a	8.45	2.5	3	b	12.7	6.0
	refired 5x	6	b	14.0	7.5	17.1	8.9	5	b	14.6	4.2	4	b	12.9	7.9
D-2 900	once	5	a	31.4	55.	57.7	18.	4	a	35.7	6.4	4	e peak	28.0	9.2
	refired 5x	6	b	23.6	4.5	103.	24.	4	a	22.4	3.6	4	e peel	22.4	3.6
D-2 1000	once	4	b	30.0	3.1	108.	32.	6	b	29.2	4.8	6	a	65.5	17.
	refired 5x	5	b	23.6	4.1	97.	5.8	5	b	26.0	9.1	5	c	146.	20.
E-1	once	6	a	42.7	20.	31.4	42.	6	a	38.6	27.	6	a	29.2	35.
	refired 5x	5	a	15.2	22.	12.7	46.	6	a	21.3	34.	4	e peak	15.6	26.
E-2	once	5	a	12.5	74.	33.8	110.	6	a	14.2	31.	5	d	17.5	9.1
	refired 5x	4	a	33.5	64.	7.97	14.	3	b	19.6	0.0	6	b	14.0	2.2

Table 6. Continued.

Ink	Fired	A			B			C			D		
		N	Mode	IX	V %	N	Mode	IX	V %	N	Mode	IX	V %
F-1	once	6	a	21.2	42.	3	e peak e peel	17.6 12.9	36. 6.3	6	a	22.0	45.
	refired 5x	4	a	10.6	34.	6	b	8.3	3.6	4	b/e	10.7	8.0
F-2	once	3	a	16.9	20.	6	a	16.4	24.	6	a	15.8	75.
	refired 5x	3	b	11.9	9.2	6	b	8.7	9.3	4	a	16.6	27.
F-3	once	6	b	21.0	22.	6	b	12.1	16.	6	b	16.4	9.6
	refired 5x	6	b	20.2	11.	4	b	25.4	14.	6	b	25.6	5.3
G-1	once	6	a	22.7	28.	3	a	37.6	27.	6	c	36.0	19.
	refired 5x	6	a	18.3	45.	5	a	28.9	13.	6	a	19.3	42.
G-2	once	4	a	18.2	26.	5	a	15.3	41.	5	a	8.94	22.
	refired 5x	4	a	9.82	45.	3	e/b peel	23.8	42.	5	a	8.56	23.
H-1	once	5	c	118.	32.	3	b	38.6	4.0	5	a	88.6	12.
	refired 5x	4	a	107.	12.	5	c	94.6	8.9	6	c	131.	8.7
										3	a	64.	25.
										4	b	26.2	11.

of adhesion analysis is true extended peel which has been designated here as mode "b". See Fig. 4(c)-3, and the corresponding part (3) of the load-elongation curve, Fig. 4(b). It can be noted from the data to follow that the data scatter for b-type failures reported as the coefficient of variation, V, expressed in percent, is usually less than 10, where

$$V = \frac{\sigma}{\bar{X}} (100) \text{ and} \quad (8)$$

$\bar{X}$  is the arithmetic mean of the data points,  $X_i$ . The standard deviation,  $\sigma$ , is determined from

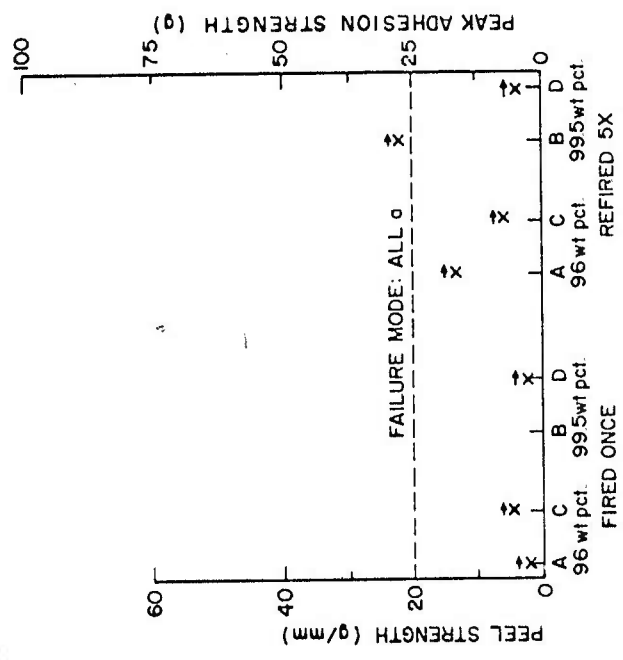
$$\sigma = \frac{\sqrt{\sum_{i=1}^{i=n} (\bar{X} - X_i)^2}}{N - 1} \quad (9)$$

where N is the number of data points.

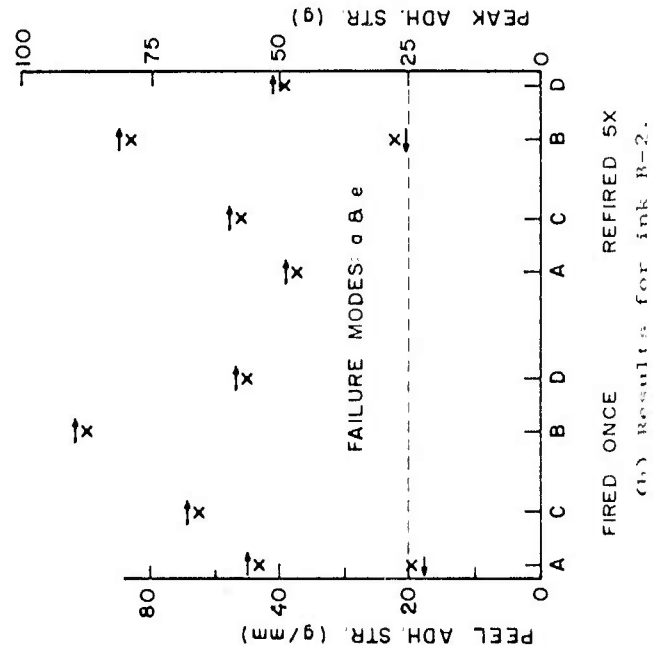
Of the six bonds planned for testing, if three or more "b" failure modes were noted, they were used in preference to any others. If any of the other failure modes were in the majority for a sample, they were the mode reported. Peel data from b, d, and e mode failures were sometimes combined, but this is described in Table 6 by ratios of data used; i.e., if 4 e's and 2 b's were used,  $N = 6$ , mode = e/b, and ratio = 2.

Another failure mode, previously noted,<sup>71</sup> occurred when the bonded area of the fired conductor land lifted, but no peel value could be ascertained. The only data of any value for these tests is the peak force required to cause failure (see Fig. 4(c)-1). This is mode "a". Because there appears to be a strong contribution of cohesion affecting the value of an a-mode failure, it is not possible to simply equate the peak load to a peel strength by some constant. In the graphical presentation to follow, whether a data point is a peel or a peak value can be distinguished by whether the accompanying arrow points to the left- or to the right-hand axis, respectively.

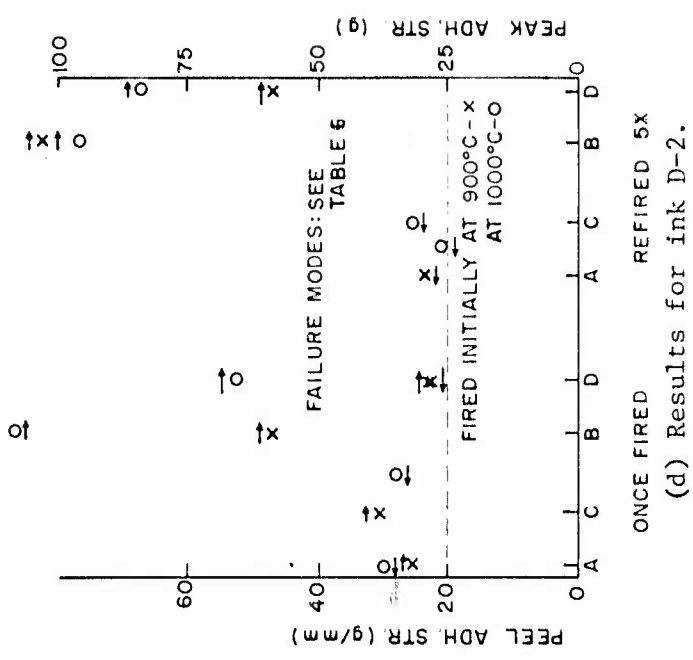
Three other modes of failure were seen to a limited extent. Where inspection of the failed parts revealed no removal of the ink from the substrate, the failure was designated a "c" mode or gold-gold failure. Data from these are referred to the peak scale. For "d" and "e" failure modes,



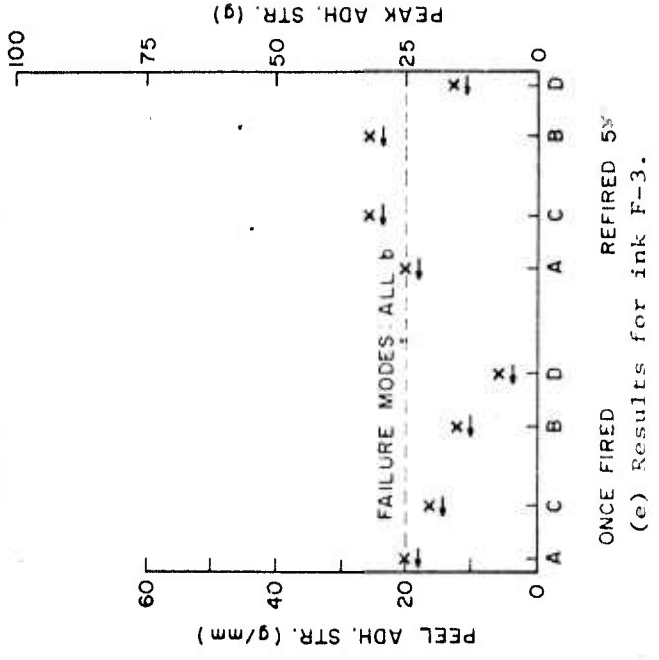
(a) Results for ink A-1.



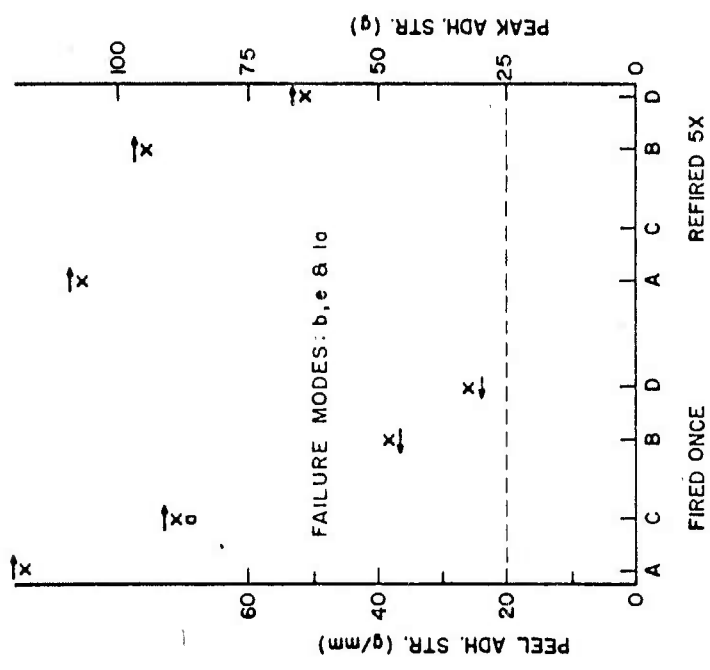
(b) Results for ink B-2.



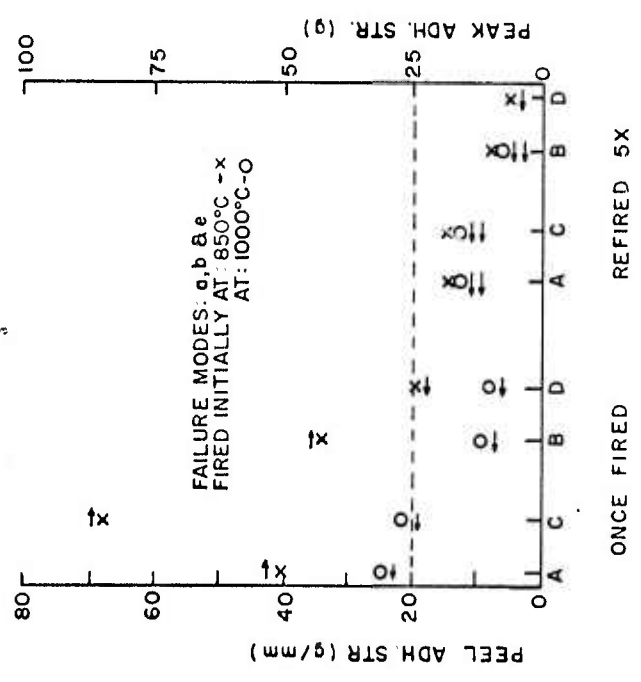
(d) Results for ink D-2.



(e) Results for ink F-3.

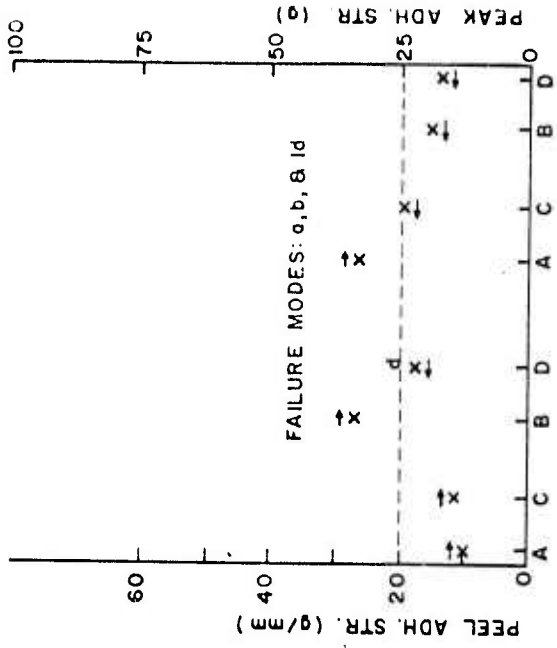


(f) Results for ink H-1.

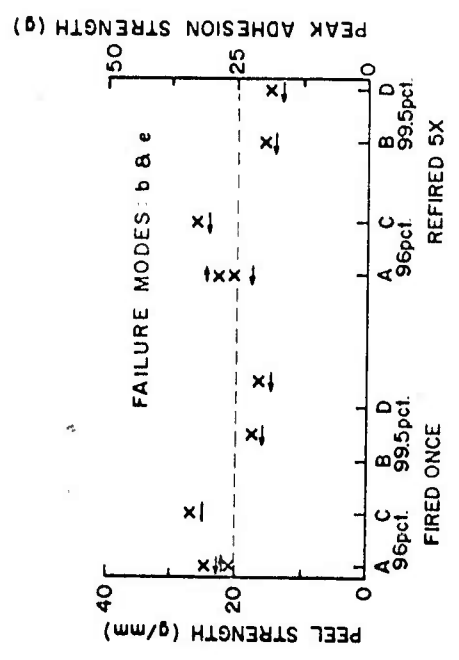


(c) Results for ink C-1.

Figure 6. Peel adhesion test results for gold inks containing substantial amounts of copper.

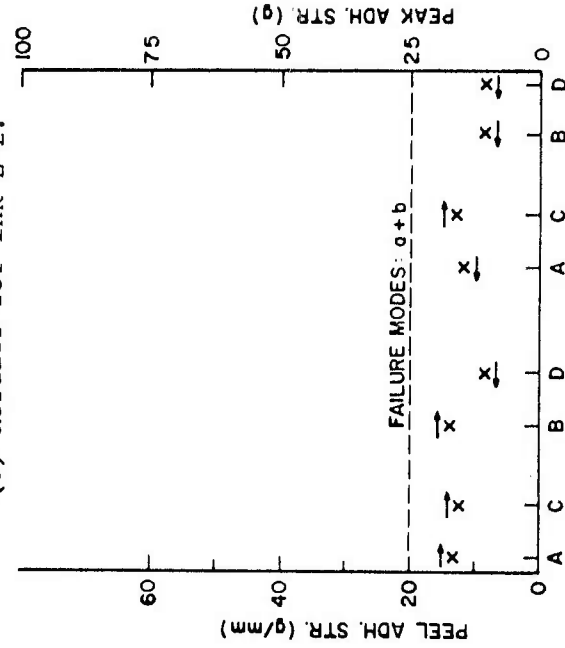


(a) Results for ink A-2.

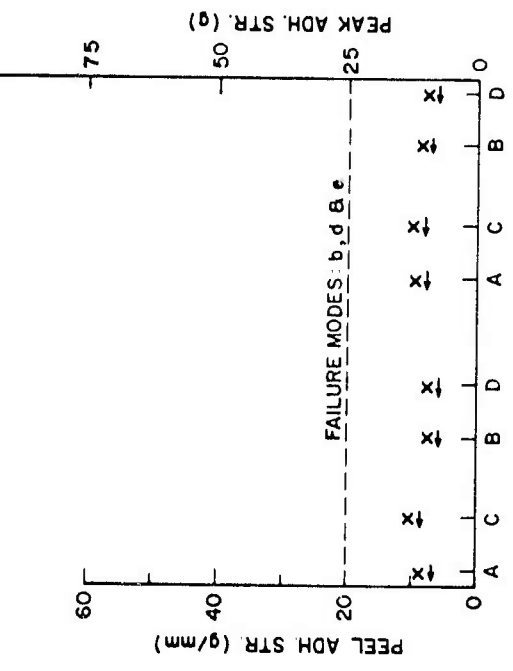


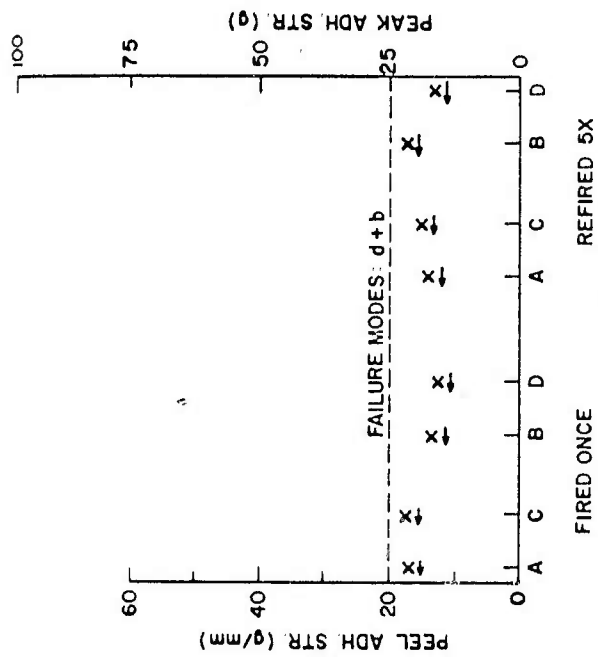
(b) Results for ink C-3.

(e) Results for ink E-2.

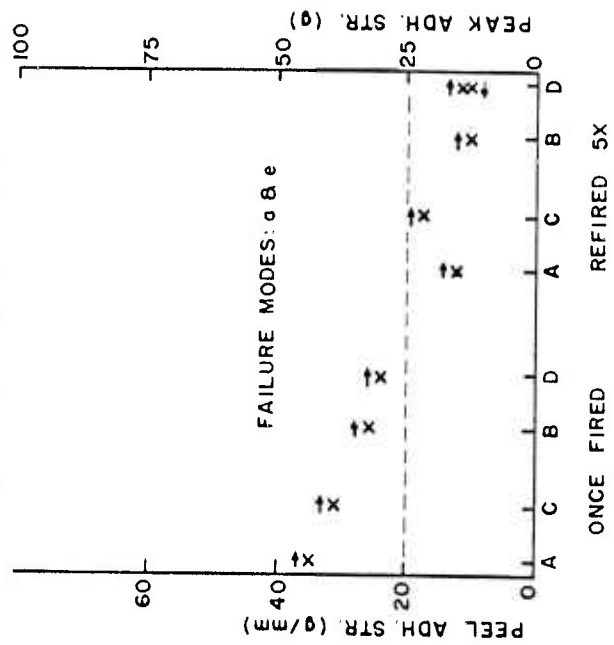


(f) Results for ink F-2.

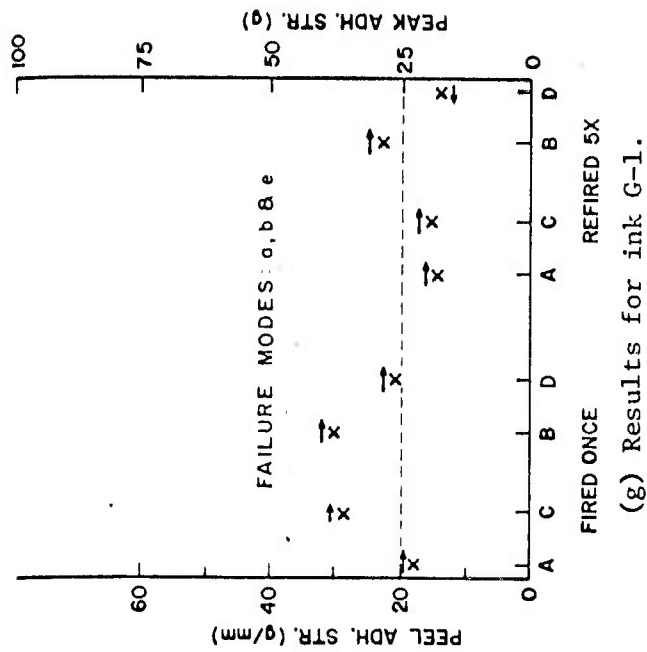




(c) Results for ink D-1.



(d) Results for ink E-1.



(g) Results for ink G-1.

Figure 7. Peel adhesion test results for frit-bonded gold inks containing 90 to 97 wt pct gold.

very short peels were obtained. The strengths reflected by these peel stresses appeared to agree quite well with "b" data on the same substrate. The difference between "d" and "e" failure modes is that the peak stress which preceded the peel was higher or lower, respectively, than the peel load itself. For these samples, both peel and peak data are shown. Peak load data, as expected, are quite scattered, with V commonly 30 percent or more. Most samples exhibited load drops (Fig. 4(c)-2), but those data have not been recorded in this report.

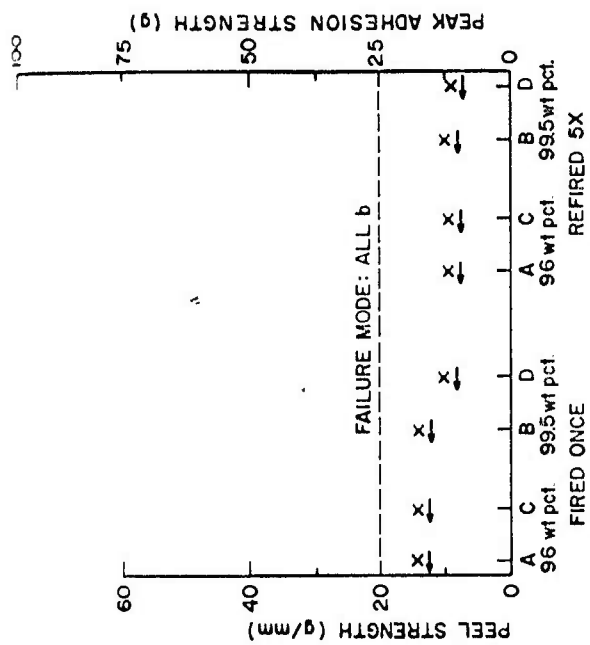
For graphical presentation the adhesion data from the several inks, substrates, and firings have been arranged into the same groups as for sheet resistance presentation. If one arbitrarily takes the horizontal line at 20 g/mm peel strength and 25 g peak strength as a base line for preliminary discussions of relative adhesion strengths, one can quickly see from Fig. 6 that about half of the reactively bonded and mixed bonded conductors surpass this level. Some combinations of substrate, ink, and firing have adhesion strengths which surpass it by very great amounts. Inks H-1, B-2, and D-2 appear to be the most adherent. Ink C-1 (initially fired at 850°C) seems to be the only ink of the group with its adhesion brought below the 20 g/mm peel line by refiring. Inks A-1 and F-3, on the other hand, seem to have had their adhesion increased by refiring.

The adhesion test data for the frit-bonded inks is shown in Fig. 7. With reference again to the adhesion base line at 20 g/mm peel and 25 g peak load, the data from all this group fell near the line. Only the data from C-3, D-1, and F-2 were clearly and completely below the line. The adhesion of ink E-1 seemed to be most strongly affected by refiring. Inks E-1 and A-2 appeared most clearly to be more adherent to 96 wt pct alumina substrates than the 99.5 wt pct materials.

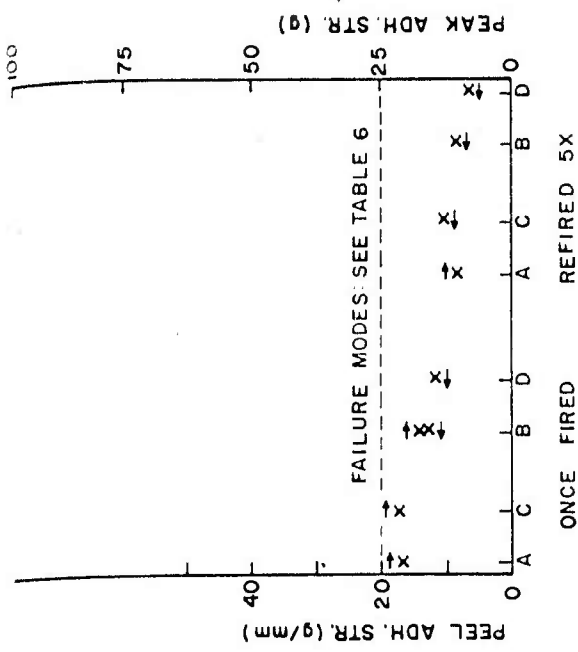
The adhesion data of the last group of inks is shown in Fig. 8. Surprisingly, even the heavily frit-loaded ink F-1 showed poor adhesion. In general, the data lay at approximately half the height of our arbitrary line.

#### D. INK SOLIDS STUDY

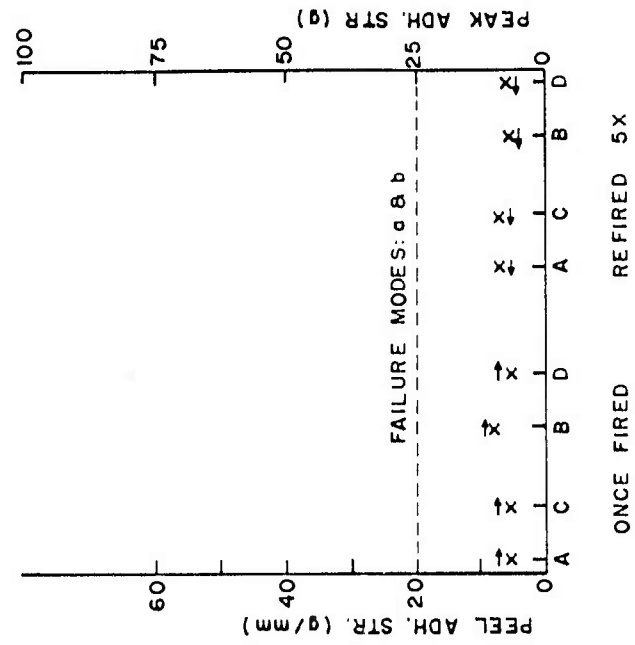
SEMographs of the dried ink solids are shown in Figs. 9 through 25. The specimen tilt shown is the angle between the beam and the perpendicular to the SEM sample holder surface. The powder mounting method is also noted.



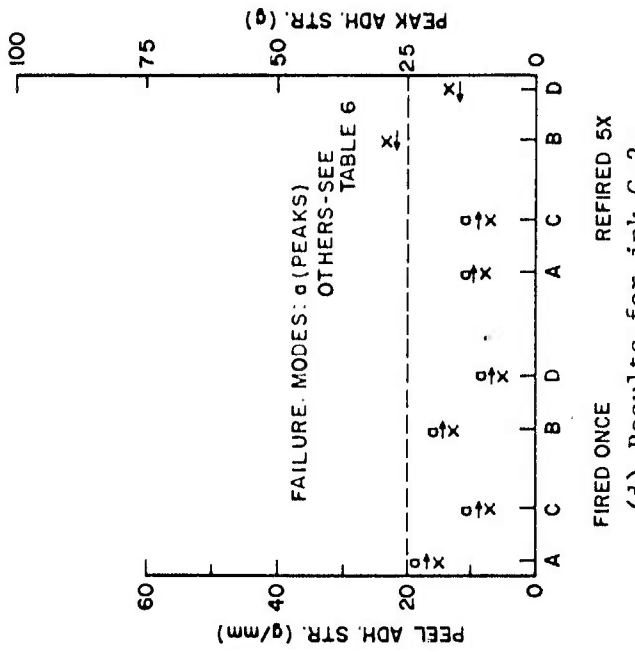
(a) Results for ink B-1.



(c) Results for ink F-1.



(b) Results for ink C-2.



(d) Results for ink G-2.

Figure 8. Peel adhesion test results for frit-bonded gold inks other than those containing 90 to 97 wt pct gold.

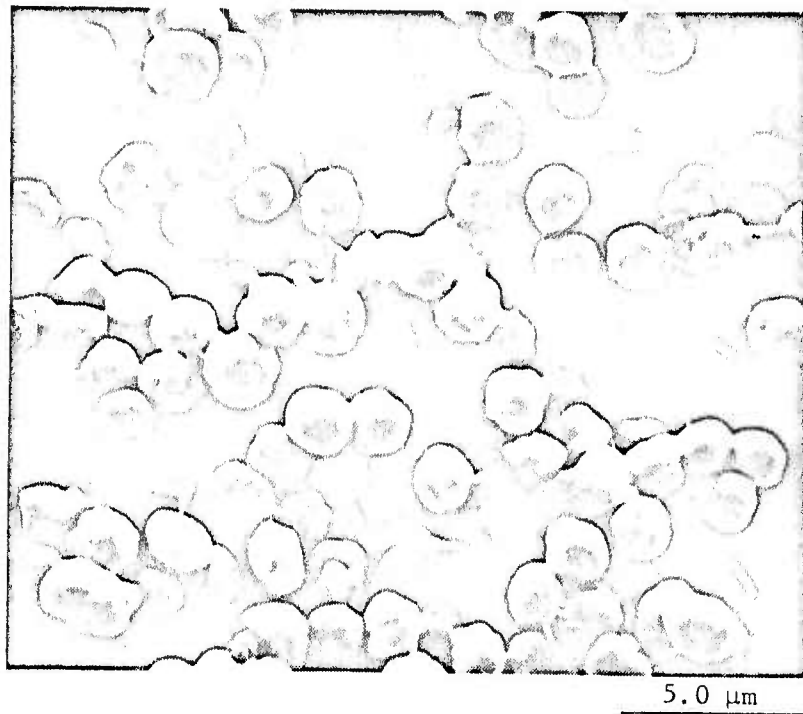


Figure 9. SEMograph of inorganic solids from ink A - 1. Specimen tilt is  $15^{\circ}$ . Prepared by method 1.

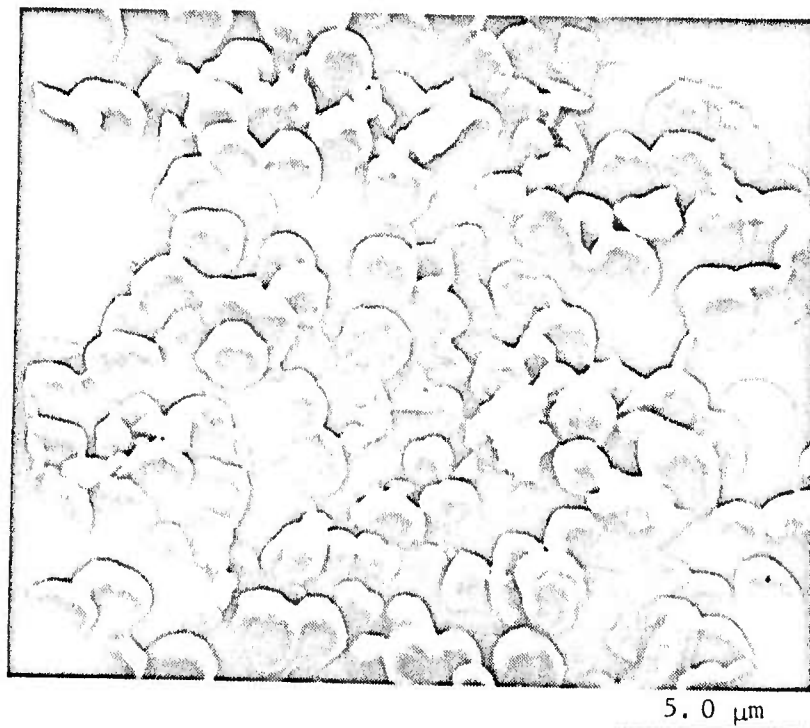
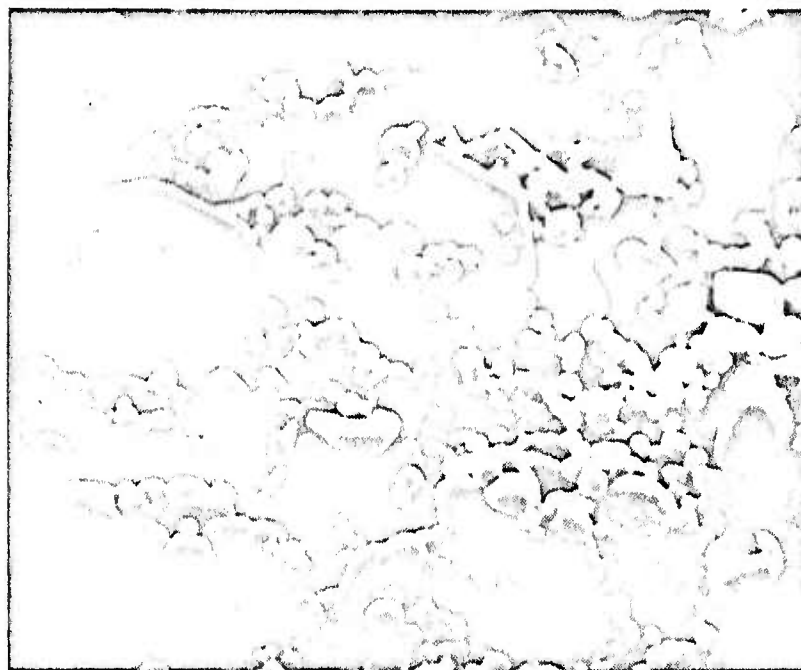


Figure 10. SEMograph of inorganic solids from ink A - 2. Specimen tilt is  $15^{\circ}$ . Prepared by method 1.



5.0  $\mu\text{m}$

Figure 11. SEMograph of inorganic solids from ink B - 1. Specimen tilt is  $15^{\circ}$ . Prepared by method 1.



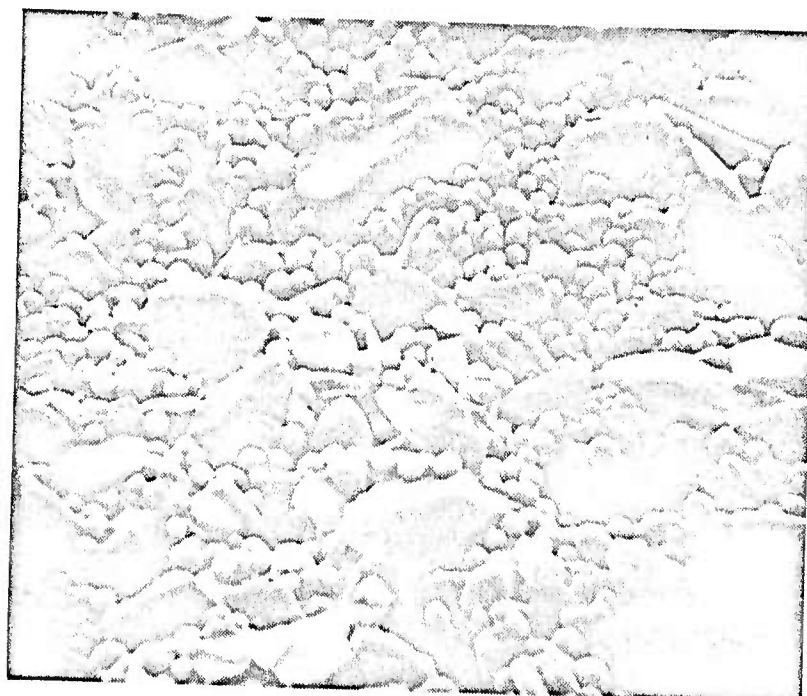
5.0  $\mu\text{m}$

Figure 12. SEMograph of inorganic solids from ink B - 2. Specimen tilt is  $15^{\circ}$ . Prepared by method 2.



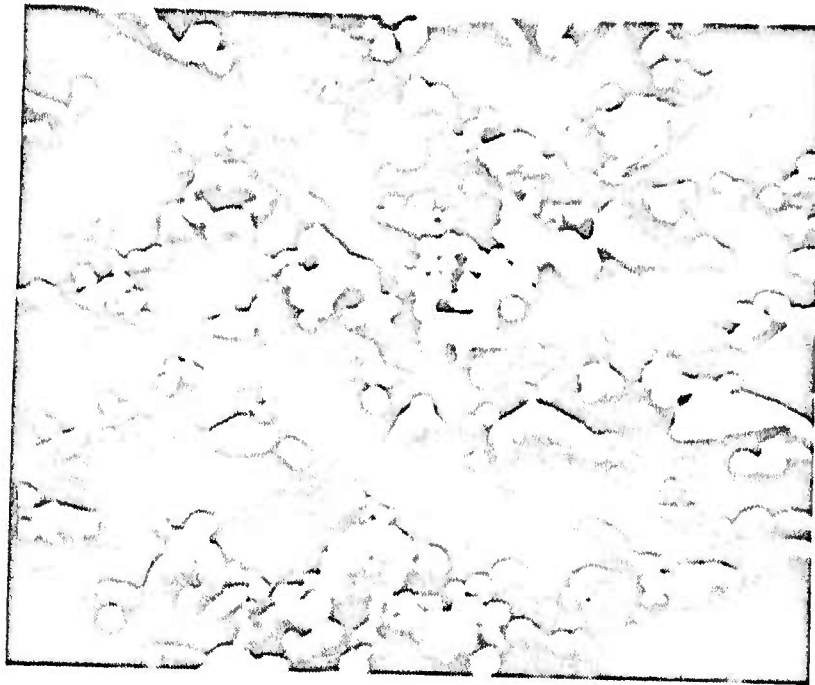
5.0  $\mu\text{m}$

Figure 13. SEMograph of inorganic solids from ink C - 1.  
Specimen tilt is  $15^{\circ}$ . Prepared by method 2.



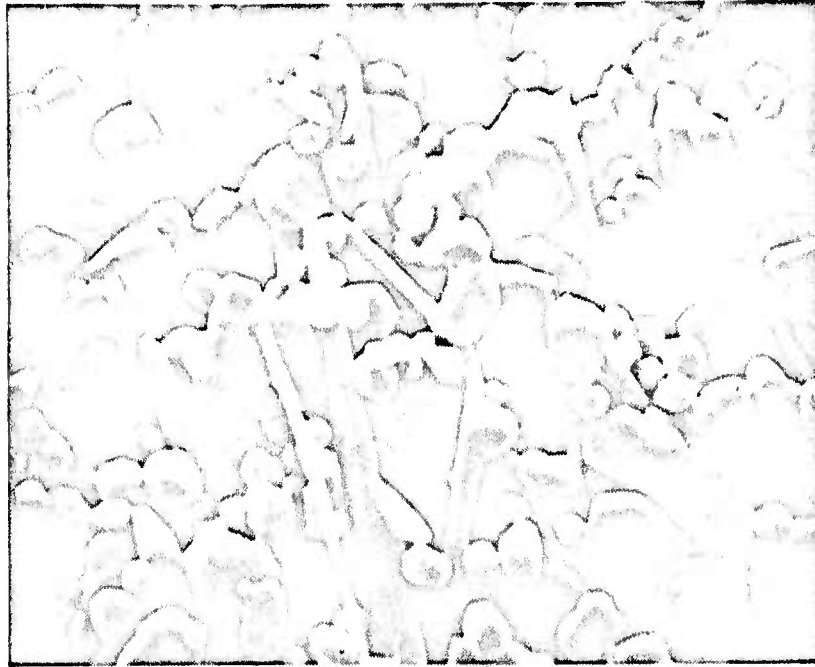
5.0  $\mu\text{m}$

Figure 14. SEMograph of inorganic solids from ink C - 2.  
Specimen tilt is  $45^{\circ}$ . Prepared by method 1.



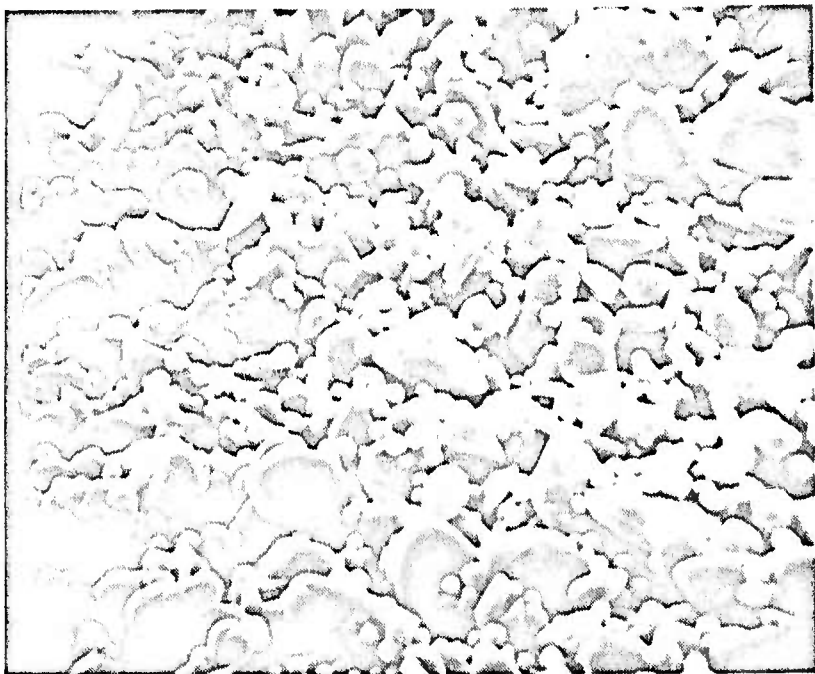
5.0  $\mu\text{m}$

Figure 15. SEMograph of inorganic solids from ink C - 3.  
Specimen tilt is  $15^{\circ}$ . Prepared by method 2.



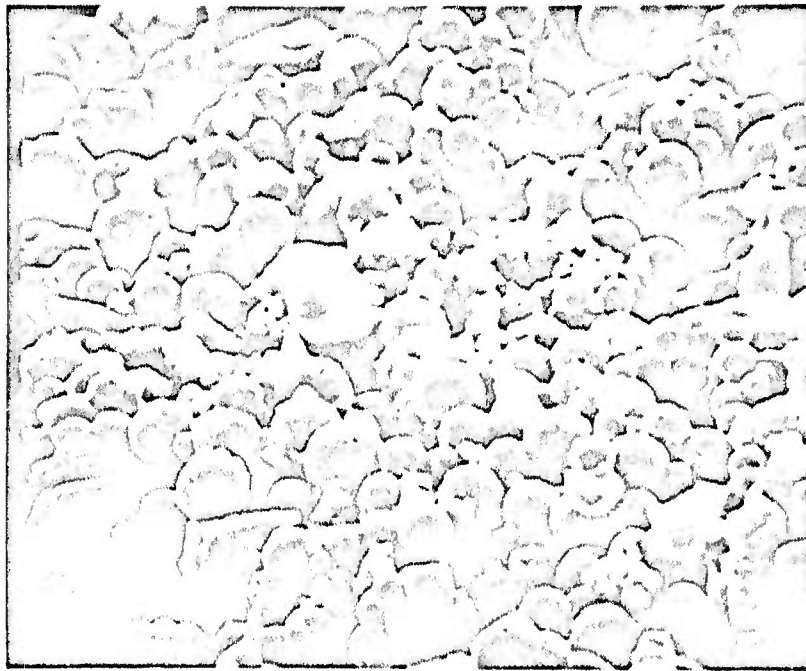
5.0  $\mu\text{m}$

Figure 16. SEMograph of inorganic solids from ink D - 1. Specimen tilt is  $15^{\circ}$ . Prepared by method 2.



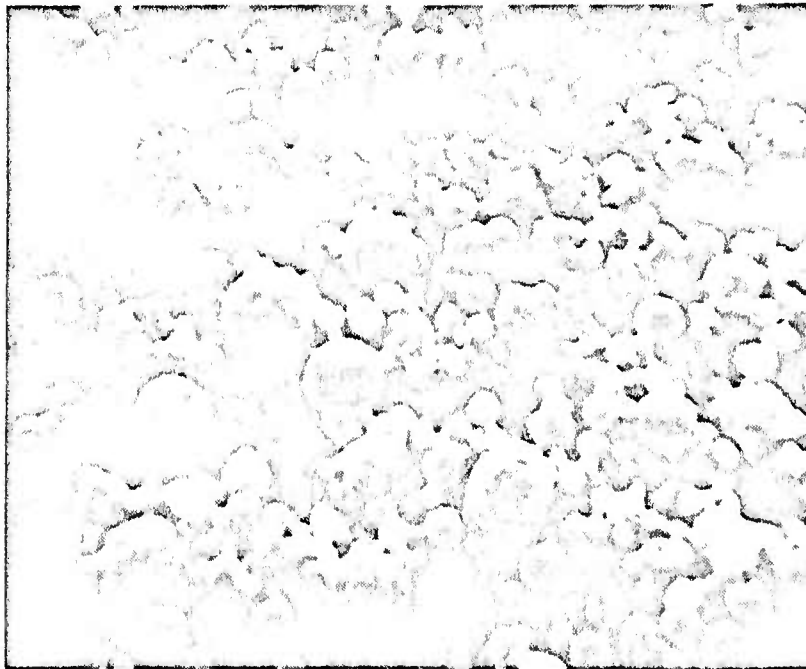
5.0  $\mu\text{m}$

Figure 17. SEMograph of inorganic solids from ink D - 2. Specimen tilt is  $15^{\circ}$ . Prepared by method 1.



10.0  $\mu\text{m}$

Figure 18. SEMograph of inorganic solids from ink E - 1.  
Specimen tilt is  $45^{\circ}$ . Prepared by method 1.



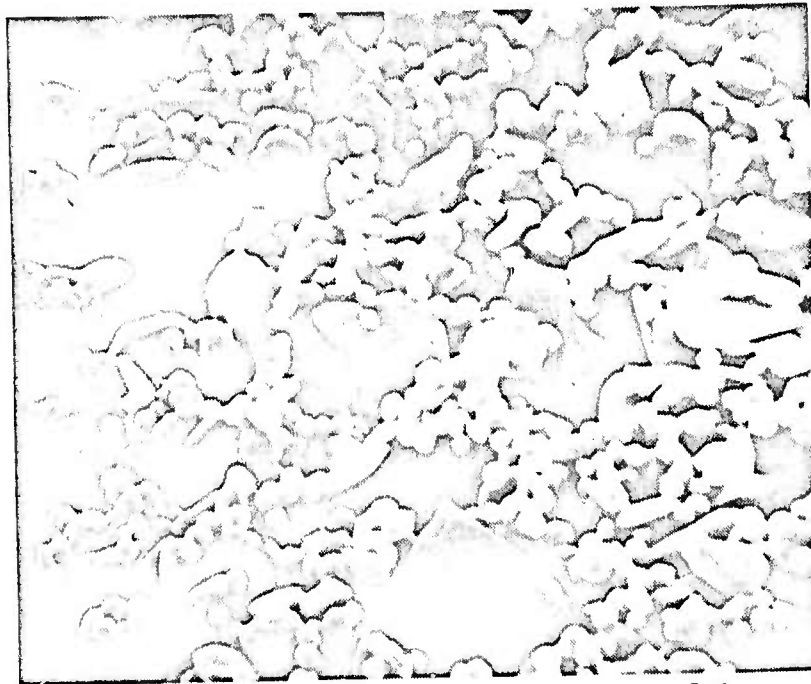
5.0  $\mu\text{m}$

Figure 19. SEMograph of inorganic solids from ink E - 2.  
Specimen tilt is  $15^{\circ}$ . Prepared by method 2.



5.0  $\mu\text{m}$

Figure 20. SEMograph of inorganic solids from ink F - 1. Specimen tilt is  $45^\circ$ . Prepared by method 1.



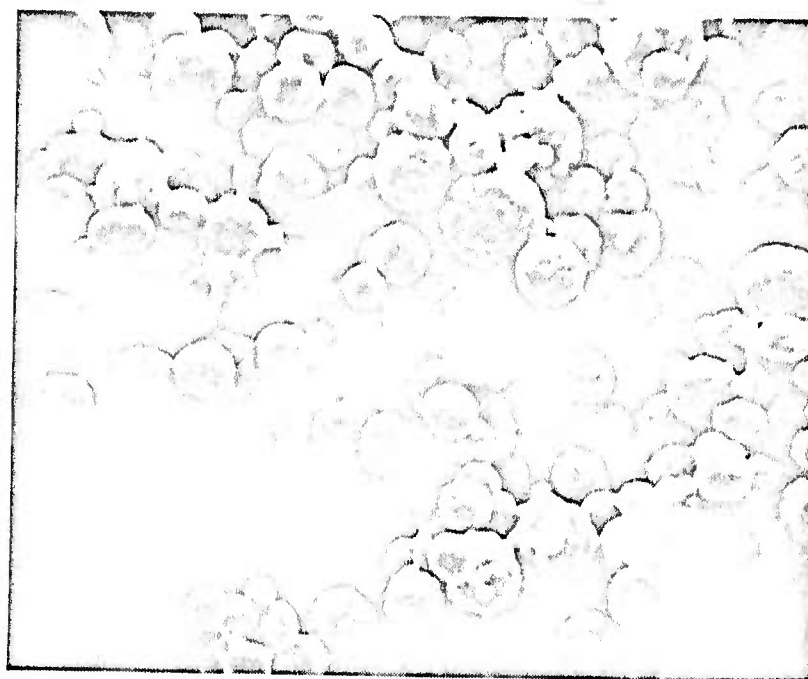
5.0  $\mu\text{m}$

Figure 21. SEMograph of inorganic solids from ink F - 2. Specimen tilt is  $45^\circ$ . Prepared by method 1.



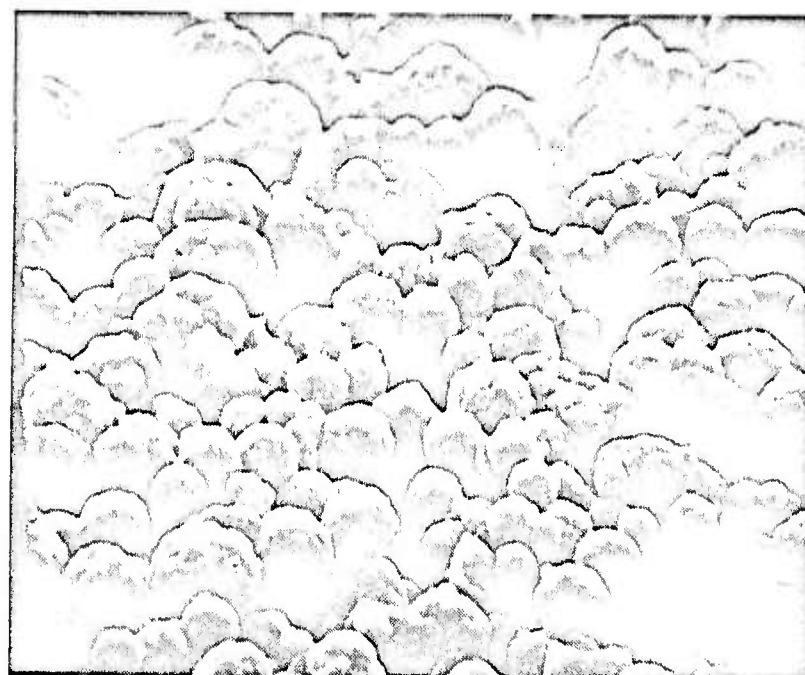
5.0  $\mu$ m

Figure 22. SEMograph of inorganic solids from ink F - 3.  
Specimen tilt is  $45^{\circ}$ . Prepared by method 1.



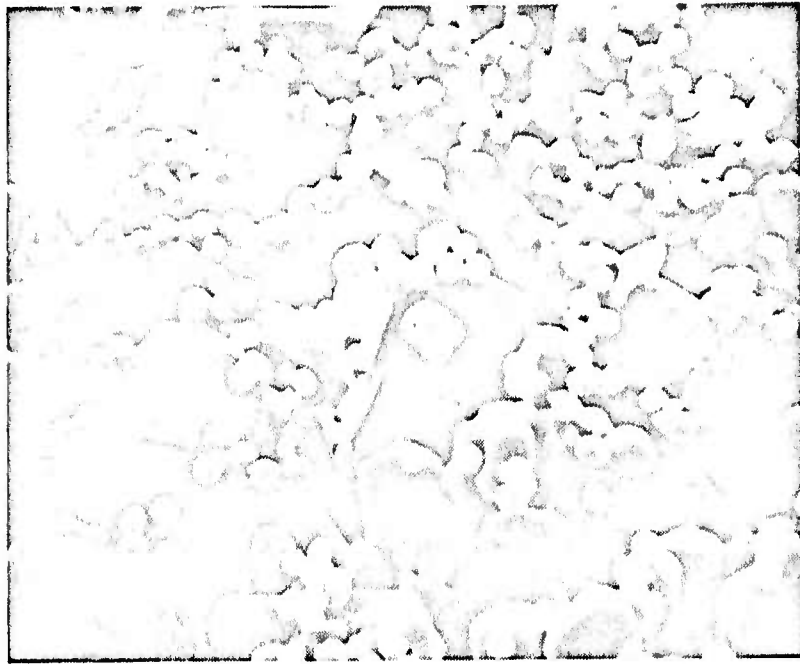
5.0  $\mu\text{m}$

Figure 23. SEMograph of inorganic solids from ink G - 1. Specimen tilt is  $15^{\circ}$ . Prepared by method 1.



5.0  $\mu\text{m}$

Figure 24. SEMograph of inorganic solids from ink G - 2. Specimen tilt is  $45^{\circ}$ . Prepared by method 1.



5.0  $\mu\text{m}$

Figure 25. SEMograph of inorganic solids from ink H - 1.  
Specimen tilt is  $15^{\circ}$ . Prepared by method 2.

The SEMographs have been grouped by the ink manufacturers, although the grouping used for sheet resistance and adhesion data presentation would have had its merits.

Figures 9 and 10 show the inks of manufacturer A. The gold powder is a uniform-size, spherical shape with diameter  $\sim 1.5 \mu\text{m}$ .

Figures 11 through 15 show the ink solids of materials from manufacturers B and C. The gold powder particles in inks B-1, B-2, C-1, and C-2 appear to be quite similar and are probably the very popular mixed hexagonal and triangular platelets and smaller sphere powder MB-1. Some of the non-gold matter of ink B-2 is suspect since oxygen burnoff problems were noted with that ink.<sup>64</sup> Ink C-3 may contain the same gold powder as the rest of manufacturer C's inks, but that is not altogether obvious. Inks D-1 and D-2 use gold powders similar to MB-1. Acicular particles, presumed to be  $\text{Bi}_2\text{O}_3$ , appear prominent in Fig. 16(D-1), while Fig. 17 for the mixed bonding ink D-2 shows little else besides the gold.

Inks E-1 and E-2 shown in Figs. 18 and 19 have spherical gold particles of  $\sim 5 \pm 3 \mu\text{m}$  diameter and  $\sim 1/2$  that, respectively. The glass of E-1 appears to have a larger particle size than that of E-2. The proportional difference appears to be greater than that of the gold sphere sizes.

Figures 20, 21, and 22 show the ink solids of F-1, F-2, and F-3. These also appear to use a gold powder similar to MB-1. Large quantities of big glass particles are obvious in F-2. F-3 shows no foreign matter, as might be guessed on the basis of Tables 2 or 3.

Figures 23 and 24 are of inks G-1 and G-2, and glass is visible in both. The spherical gold powder(s) in these inks appear(s) to be similar to MG-2. Ink H-1, shown in Fig. 25, appears to utilize MB-1 or a similar gold powder. As has been observed for reactively bonding inks, little besides gold is visible in the ink solids.

#### E. DISCUSSION OF RESULTS - PROPERTIES OF THE INKS STUDIED

Comments on the properties of the inks and substrates evaluated must be somewhat preliminary since the data are not complete. However, certain statements can be made.

If we treat the reactively bonded inks first, there are really only two - F-3 and H-1. Since it contains only copper oxide as a bonding agent,

F-3 cannot achieve good adhesion strength by firing at the recommended temperatures.<sup>72</sup> Adhesion is projected to rise rapidly with higher temperature firings. The high-load "c" failure mode seen only with H-1, leads to two important conclusions. The first is that thermocompression bonding is not as good with this material as it should be. A good thermocompression bond will cause the strip of lead frame to rupture before the bond fails. The second is that the adhesion of the conductor to alumina is extremely resistant to reduction by the plastic flow of the thick-film gold under bonding stresses. In a fiber-structure frit-bonded conductor, plastic flow of the gold material at the bonding temperature would probably shear the brittle glass fibers and drastically reduce adhesion. The thick-film gold immediately adjacent to the ceramic-to-thick film conductor interface will undergo very little shear strain (it is in the boundary layer) and therefore should not disrupt any chemical bonding<sup>72</sup> across that interface. It should be noted that there is great interest in lead frame bonding to the H-1 material, and that its bondability can be increased by etching with ammonium persulphate.<sup>72</sup>

The mixed-bonded materials, A-1, B-2, C-1, and D-2, are the newest class of gold conductors. Preliminary study of a few of these with crossed-polarized light have indicated that some of them can demonstrate very low proportions of glass and other foreign material on the as-fired conductor surface, suggesting excellent bondability. Since they also demonstrated reasonable adhesion and good conductivity in most cases, they appear to be a useful innovation in gold thick-film conductors.

The frit-bonded inks behaved approximately as expected, with a few exceptions. If one considers low sheet resistance and good adhesion strength after one or several firings to be the principal requirements for gold conductor inks, the materials A-2, E-1, E-2, and G-1 all performed satisfactorily. (It should be noted that all of these contain spherically shaped gold powder.) The frit-bonded inks with low frit contents, B-1 and C-2, showed low adhesion strengths as indicated.

The inks with the highest proportions of glasses, F-1 and F-2, had rather poor adhesion. This would tend to contradict our preliminary model in which added frit would yield increased adhesion.<sup>64</sup> It was noted, how-

ever, that the frit had extensively flowed away from the conductor pattern onto the alumina for both these conductors. Clearly, if the glass is not a part of the conductor land, it can do little to improve adhesion of the metal phase. Interestingly, the manufacturer of these pastes has recently introduced a number of new thick-film conductors for which improved properties are claimed.

In passing it should be noted that ink C-2, which is advertised as being firable in hydrogen, was useless after such firing in our experiments. Discussions with the manufacturer produced the recommendation for a two-step firing in which the first firing is oxidizing at modest temperatures for binder burnout, and the second firing is in hydrogen.

As noted earlier in the report the discussion here is incomplete. Measurements now under way of land cross sections of the peel and resistance patterns (by profilometry using a stylus-type instrument) are required to fully rationalize the adhesion and resistance data presented here. Microstructural evaluations are expected to put much of the frit-bonded ink data into better perspective. Consideration of the reactively loaded and mixed-bonded inks has only begun. Much more study is anticipated before these last two classes of materials can be fully understood.

#### IV. WORK TO BE DONE IN THE NEXT PERIOD

The work planned for the next quarter falls into four principal groups: finishing the first parametric study; starting the second; evaluating adhesion test methods, in theory and in practice; and pursuing the model ink program.

It is anticipated that evaluation of the four substrates by physical and chemical techniques will be completed in the coming quarter except for the use of specialized surface analysis techniques such as scanning Auger spectrometry. Considerable effort will be put into the analysis of adhesion-producing phase microstructures by mercury vapor leaching and SEM and by crossed-polarized light. Bulk conductivities will be determined for some of the ink-substrate-firing combinations. Completion of these will end the primary parametric study.

Selection of materials for the second study is nearly complete. As soon as the materials required are received, that work will begin.

Study of adhesion test methods is well under way. A report on several physical testing methods, and theoretical evaluations of those methods will be made in the next quarterly report.

The model ink program has also begun. Gold powders and vehicles were received in the first quarter.<sup>64</sup> Preliminary work on glass melting and fritting has been accomplished in this quarter. Work will be increased on the model ink program in the next period.

In general, the work of the third quarter should lead to a much more fundamental understanding of the behavior of some of the newer inks. The number of commercial gold thick films introduced in the last two or three years is quite large, and some of the more interesting innovations, particularly the mixed-bonded inks, have received very little study of the mechanisms of adhesion.

## APPENDIX A

### DETAILS OF EXPERIMENTAL TECHNIQUE

#### 1. Fabrication of Gold Lead Frames

Gold foil of 99.9 wt pct purity, 0.002 in. thick x 4 in. wide x 5½ in. long, was degreased in trichlorethylene vapor and wiped with cotton swabs wet with acetone. The foils were dipped in Kodak KMER photoresist which had been thinned one-to-one with KMER thinner. The foils were initially dried in a filtered air, laminar flow hood at room temperature for 20 minutes. The resist was fully hardened for 15 minutes in a circulating air oven at 100°C. Contact print exposure of the photoresist-coated gold against a pattern of 35 lead frames on 4 in. x 5 in. Estar-based Kodak high resolution film was performed with a Co-Light Model DMVL Contact Printer for 2½ min., simultaneously exposing the photoresist on both sides of the gold foil. KMER developer was sprayed onto the film using an air-brush for 7½ min.

After blowing the foils dry with nitrogen, they were placed in a potassium iodide and iodine-type etchant C-35 (Film Microelectronics, Burlington, Mass.). The bath was under constant agitation with a magnetic stirrer and was at room temperature. Typical etching times were about one hour. When etching was complete, the remaining KMER resist was stripped at 100°C with Resist Strip J-100, Indust-Ri-Chem Labs (Richardson, Texas). All residues were removed from the now completed gold lead frames with several rinses of Mallinckrodt Transist-Ar grade methylethyl ketone. The frames were allowed to dry on Kimberly Clark Kimwipe tissues.

#### 2. Test Substrate Printing

Substrates were printed with a Microcircuit Engineering (Mt. Holly, N. J.) 280 mesh, 0.0012 in.-diameter wire stainless steel screen with a 0.001 in.-thick emulsion build-up on the substrate side of the screen. The screens were mounted on a standard 8 in. x 10 in. precision-machined aluminum frame. Printing was accomplished with an Aremco Model 3100 screen printer modified to accept the frame of the screen. This printer is equipped with solid micrometer stops for snap-off and squeegee compression adjustment. The

squeegee speed and cycle time are controlled by an air-oil cylinder and a motor-driven cam programmer, respectively. A built-in squeegee stroke timer was available to assist in establishing the best squeegee speeds.

The substrate nest and printing squeegee were adjusted for parallelism to the screen such that a 0.001 in. change in squeegee compression would make the difference between no print and a complete print of the pattern.

Printing was begun with a 0.020 in. snap-off distance (undeflected screen-to-substrate separation), a squeegee speed of 5.1 in./sec, and a squeegee compression of 0.010 in. Squeegee compression and snap-off distance were increased slightly a few times to maintain screen tension during the printing of the more than 1000 pieces. The squeegee was polyurethane with a durometer hardness of 80 and a 45° attack angle.

Noticeable characteristics of the 17 inks (including tendency to string, ability to hold definition of screened pattern after firing, other rheological characteristics, and the ability to withstand prolonged screening time without losing printability) are described in Table 4 of the main text. All thinning was done with the recommended thinner, which was used sparingly. After printing, the patterns were allowed to stand for a minimum of 15 minutes at room temperature and were dried in an oven at either 125 or 150°C for varying times as recommended by the manufacturer. Because adhesion testing was the most important intended use of the substrates, maximum emphasis was given to the printing of five acceptable 0.020 in.-wide conductor lands.

### 3. Substrate Firing

The screened ink patterns were fired in a BTU Engineering Corporation (Waltham, Mass.) VQ-2 series thick-film firing furnace. The unit is equipped with five heating zones and four controllers and has an indicated temperature control capability of  $\pm 1/2^\circ\text{C}$ . Four flat top profiles with peak temperatures of 850°, 900°, 950°, and 1000°C (Fig. 3 in the main text) with a 3 in./min. belt speed provided approximately 10 min. at peak temperatures. These met the ink manufacturers' requirements for air atmosphere initial firings and refirings. Ten pieces of each matrix group were given the

metallizer firing suggested by the manufacturer. Five pieces of the ten were then refired with two firings at the temperature necessary to fire a compatible crossover dielectric. This was followed with three more firings at the temperature necessary to fire a compatible resistor composition.

In the cases where a choice of several dielectric and resistor firing temperatures were available from the manufacturer, the ones used were those judged to be either the most typical or the most generally useful to military hybrid work.

## REFERENCES

1. R. W. Berry, P. M. Hall and M. T. Harris, Thin Film Technology, (D. Van Nostrand Co., Inc., Princeton, N.J., 1968).
2. L. I. Maissel and R. Glang, Handbook of Thin Film Technology, (McGraw Hill Book Co., New York, 1970).
3. L. V. Gregor, "Thin Film Processes for Microelectronic Application," Proc. IEEE 59, No. 10, pp. 1390-1403 (1971).
4. D. M. Mattox, "Thin Film Metallization of Oxides in Microelectronics," Thin Solid Films 18, No. 1, pp. 173-186 (1973).
5. J. L. Vossen, "Control of Film Properties by rf-Sputtering Techniques," J. Vac. Sci. Technol. 8, No. 5, pp. S12-30 (1971).
6. B. N. Chapman, "Thin Film Adhesion," J. Vac. Sci. Technol. 11, No. 1, pp. 106-113 (Jan./Feb. 1974).
7. D. G. Williams, "The Adhesion of Vacuum-Deposited Films," RFP-1690 Dow Chemical Co. to USAEC Contract No. AT (29-1)-1106 (1972).
8. N. M. Poley and H. L. Whitaker, "Adhesion of Chromium Films to Soda Lime Glass," J. Vac. Sci. Technol. 11, No. 1, pp. 114-118 (Jan./Feb. 1974).
9. R. Jacobsson and B. Kruse, "Measurement of Adhesion of Thin Evaporated Films on Glass Substrates by Means of the Direct Pull Method," Thin Solid Films 15, No. 1, pp. 71-77 (1971).
10. D. M. Mattox, "Influence of Oxygen on the Adherence of Gold Films to Oxide Substrates," J. Appl. Phys. (USA) 37, No. 9, pp. 3613-5 (1966).
11. D. G. Moore and H. R. Thornton, "Effect of Oxygen on the Bonding of Gold to Fused Silica," J. Res. NBS 62, No. 3, pp. 127-135 (1959).
12. K. E. Haq et al., "Adhesion Mechanism of Gold-Underlayer Film Combinations on Oxide Substrates," J. Vac. Sci. Technol. 6, No. 4, pp. 148-152 (1968).
13. H. Graf von Harrach and B. Chapman, "Charge Effects in Thin Film Adhesion," Thin Solid Films 13, No. 1, pp. 157-161 (1972).
14. B. V. Derjaguin and V. P. Smilga, "Electronic Theory of Adhesion," J. Appl. Phys. 38, No. 12, pp. 4609-16 (1967).
15. C. A. Calow and I. T. Porter, "The Solid State Bonding of Nickel to Alumina," J. Mater. Sci. 6, No. 1, pp. 156-163 (1971).
16. C. A. Calow et al., "The Solid State Bonding of Nickel, Chromium and Nichrome Sheets to  $\alpha$ -Al<sub>2</sub>O<sub>3</sub>," J. Mater. Sci. 6, No. 1, pp. 150-155 (1971).

17. J. T. Klomp, "Bonding of Metals to Ceramics and Glasses," Amer. Ceram. Soc. Bull. 51, No. 9, pp. 683-688 (1972).
18. D. W. Hamer and J. V. Biggers, Thick Film Hybrid Microcircuit Technology, (Wiley-Interscience, New York, 1972).
19. L. F. Miller, Thick Film Technology and Chip Joining, (Gordon and Breach, Science Publishers, Inc., New York, 1972).
20. M. L. Topfer, Thick-Film Microelectronics, (Van Nostrand Reinhold Co., New York, 1971).
21. D. G. Burnside, "Ceramic-Metal Seals of the Tungsten-Iron Type," RCA Review 15, No. 1, pp. 46-61 (1954).
22. G. R. Van Houten, "A Survey of Ceramic-to-Metal Bonding," J. Amer. Ceram. Soc. 38, No. 6, pp. 301-305 (1959).
23. J. F. Clarke et al., "State-of-the-Art Review of Ceramic-to-Metal Joining," Technical Report AFML-TR-65-143, AF Materials Laboratory, Wright-Patterson AF Base, Ohio (1965).
24. W. H. Kohl, Handbook of Materials and Techniques for Vacuum Devices, (Reinhold Publishing Co., New York, 1967).
25. H. E. Pattee, "Joining Ceramics and Graphite to Other Materials," NASA SP-5052 Office of Technology Utilization, NASA, Washington, D.C. (1968).
26. H. Pulfrich, Ceramic-to-Metal Seal, U. S. Patent 2,163,407, June 20, 1939.
27. H. Pulfrich, Vacuum-Tight Seal, U. S. Patent 2,163,408, June 20, 1939.
28. H. Pulfrich, Ceramic-to-Metal Seal, U. S. Patent 2,163,409, June 20, 1939.
29. H. Pulfrich and R. Magner, Ceramic-to-Metal Seal, U. S. Patent 2,163,410, June 20, 1939.
30. H. J. Nolte and R. F. Spurck, "Metal-Ceramic Sealing with Manganese," Television Eng. 1, No. 11, pp. 14-18 (1950).
31. S. S. Cole, Jr. et al., "Metal-to-Ceramic Seal Technology Study," RADC-TR-60-236, Rome Air Development Center, Griffiss Air Force Base, New York (1960).
32. C. I. Helgesson, "Bonding Mechanism in Molybdenum-Manganese Ceramic-to-Metal Seals," Trans. of Chalmers University of Technology, Gothenburg, Sweden, No. 2.292, pp. 3-8 (1964).
33. A. C. Grimm and P. D. Strubhar, "Dielectric to Metal Seal Technology Study," RADC-TDR 63-472, Rome Air Development Center, Griffiss Air Force Base, New York (1963).

34. P. F. Varadi and R. Dominquez, "Tungsten Metallizing of Ceramics," Amer. Ceram. Soc. Bull. 45, No. 9, pp. 789-91 (1966).
35. R. E. Cowan et al., "Mechanism of Adherence of Tungsten to Bodies Containing Yttria," Fall Meeting Amer. Ceram. Soc., Philadelphia, Pa. (Sept. 7, 1964).
36. R. E. Cowan and S. D. Stoddard, "Ceramic Materials for Nuclear Thermionic Converters," 65th Ann. Meeting, Amer. Ceram. Soc., Pittsburgh, Pa. (May 1, 1963).
37. R. E. Cowan and S. D. Stoddard, "Tungsten Metallizing Alumina-Yttria Ceramics," 66th Ann. Meeting, Amer. Ceram. Soc., Chicago, Ill. (April 22, 1964).
38. R. S. Kiwak, "Metal-to-Ceramic Seals for High Temperature Service," American Society for Metals Technical Report P10-3-64 (1964).
39. L. A. Tentarelli et al., "Low Temperature Refractory Metal-to-Ceramic Seals," Final Report ECOM-03734-F, U. S. Army Electronics Command, Contract No. DA-36-039-AMC-037345 (April 1966).
40. L. C. Hoffman et al., "Adhesion of Platinum-Gold Glaze Conductors," IEEE Trans. on Parts, Materials and Packaging, PMP-1, No. 1, pp. s-381-386 (1965).
41. W. A. Crossland and L. Hailes, "Thick Film Conductor Adhesion Reliability," Proc. International Hybrid Microelec. Symp., pp. 3.3.1-13, Beverly Hills, California (Nov. 16-18, 1970).
42. J. R. Floyd, "Effect of Composition and Crystal Size of Alumina Ceramics on Metal-to-Ceramic Bond Strength," Amer. Ceram. Soc. Bull. 42, No. 2, pp. 65-70 (1963).
43. M. E. Arthur and L. E. Fussell, "Effect of Sintering Conditions on  $Al_2O_3$ -Mo/Mn Bond Strengths," Amer. Ceram. Soc. Bull. 50, No. 12, pp. 982-984 (1971).
44. J. T. Klomp and T. P. J. Botden, "Sealing Pure Alumina Ceramics to Metals," Amer. Ceram. Soc. Bull. 49, No. 2, pp. 204-211 (1970).
45. A. G. Pincus, "Metallographic Examination of Ceramic-to-Metal Seals," J. Amer. Ceram. Soc. 36, No. 5, pp. 152-158 (1953).
46. A. G. Pincus, "Mechanism of Ceramic-to-Metal Adherence-Adherence of Molybdenum to Alumina Ceramics," Ceram. Age 63, pp. 16-20, 30-32 (1954).
47. L. H. La Forge, Jr., "Application of Ceramic Sections in High-Power Pulsed Klystrons," Amer. Ceram. Soc. Bull. 35, No. 3, pp. 117-122 (1956).

48. S. S. Cole, Jr., and F. J. Hynes, Jr., "Some Parameters Affecting Ceramic-to-Metal Seal Strength of a High-Alumina Body," Amer. Ceram. Soc. Bull. 37, No. 3, pp. 135-138 (1958).
49. S. S. Cole, Jr., and G. Sommer, "Glass-Migration Mechanism of Ceramic-to-Metal Seal Adherence," J. Amer. Ceram. Soc. 44, No. 6, pp. 265-271 (1961).
50. F. P. Denton and H. Rawson, "Metallizing of High Al<sub>2</sub>O<sub>3</sub> Ceramics," Trans. Brit. Ceram. Soc. 59, No. 2, pp. 25-37 (1960); Ceram. Abstr. p. 163e (July 1960).
51. L. Reed and R. A. Huggins, "Electron Probe Microanalysis of Ceramic-to-Metal Seals," J. Amer. Ceram. Soc. 48, No. 8, pp. 421-426 (1965).
52. G. C. Kuczynski, "Physics and Chemistry of Sintering," Advan. Colloid Interface Sci. 3, No. 1, pp. 275-330 (1972).
53. V. N. Eremenko et al., Liquid Phase Sintering, Consultants Bureau New York (1970).
54. W. D. Kingery, "Densification During Sintering in the Presence of a Liquid Phase I. Theory," J. Appl. Phys. 30, No. 3, pp. 301-306 (1959).
55. W. D. Kingery, Introduction to Ceramics, (John Wiley & Sons, Inc., New York, 1960), pp. 386-389.
56. W. D. Kingery and M. D. Narasimhan, "Densification During Sintering in the Presence of a Liquid Phase II Experimental," J. Appl. Phys. 30, No. 3, pp. 307-310 (1959).
57. S. S. Cole, Jr., "Sintering of Ag-Pd in the Presence of a Reactive Glass," J. Amer. Ceram. Soc. 55, No. 6, pp. 296-299 (1972).
58. D. L. Johnson and I. B. Cutler, "Diffusion Sintering: I. Initial Stage Sintering Models and Their Application to Shrinkage of Powder Compacts," J. Amer. Ceram. Soc. 46, No. 11, pp. 541-545 (1963).
59. R. E. Hoffman and D. J. Turnbull, "Lattice and Grain Boundary Self-Diffusion in Silver," J. Appl. Phys. 21, No. 7, pp. 632-635 (1950).
60. W. D. Kingery, "Role of Surface Energies and Wetting in Metal-Ceramic Sealing," Amer. Ceram. Soc. Bull. 35, No. 3, pp. 108-112 (1956).
61. B. C. Allen and W. D. Kingery, "Surface Tension and Contact Angles in Some Liquid Metal-Solid Ceramic Systems at Elevated Temperatures," Trans. Met. Soc. AIME 215, No. 1, pp. 30-37 (1959).
62. M. Humenik, Jr., and W. D. Kingery, "Metal-Ceramic Interactions: III. Surface Tension and Wettability of Metal-Ceramic Systems," J. Amer. Ceram. Soc. 37, No. 1, pp. 18-23 (1954).

63. J. A. Pask and R. M. Fulrath, "Fundamentals of Glass-to-Metal Bonding: VIII Nature of Wetting and Adherence," J. Amer. Ceram. Soc. 45, No. 12, pp. 592-596 (1962).
64. T. T. Hitch and K. R. Bube, "Basic Adhesion Mechanisms in Thick and Thin Films," RCA Laboratories, Contract No. N00019-74-C-0270, Quarterly Report No. 1, April 30, 1974.
65. Op. cit. Ref. 55, p. 148.
66. R. E. Honig, "Materials Characterization at RCA Laboratories," Solid State Tech. 13, No. 3, pp. 59-66 (1970).
67. R. C. Weast, ed., Handbook of Chemistry and Physics, p. B-157, (The Chemical Rubber Co., Cleveland, Ohio, 1970).
68. C. E. Wicks and F. E. Block, "Thermodynamic Properties of 65 Elements - Their Oxides, Halides, Carbides, and Nitrides," Bulletin 605 Bur. of Mines, U. S. Government Printing Office, Washington, D. C. (1963).
69. B. R. Smith and R. L. Dietz, "An Innovation in Gold Paste," Proc. Int'l. Microelec. Symp. (ISHM), pp. 2-A-5 to -8 (1972).
70. R. G. Loasby, N. Davey, and H. Barlow, "Enhanced Property Thick-Film Conductor Pastes," Solid State Tech. 15, No. 5, pp. 46-50 (1972).
71. T. T. Hitch, "Phase Morphology and Adhesion in Thick-Film Conductor Inks," Proc. Int'l. Microelec. Symp. (ISHM), pp. 7-7-1 to -11 (1971).
72. T. T. Hitch, "Adhesion, Phase Morphology, and Bondability of Reactively-Bonded and Frit-Bonded Gold and Silver Thick-Film Conductors," presented at the AIME Symposium, Preparation and Properties of Electronic Materials, Las Vegas, Nev., August 27-29, 1973, published in J. Elec. Materials 3, No. 2, pp. 553-577 (1974).